

UNCLASSIFIED

AD NUMBER

ADB171686

LIMITATION CHANGES

TO:

Approved for public release; distribution is unlimited.

FROM:

Distribution authorized to DoD only;  
Proprietary Information; 10 SEP 1992. Other  
requests shall be referred to Army Medical  
Research and Development Command, Fort Detrick,  
MD 21702.

AUTHORITY

USAMRDC ltr 3 Oct 1994

THIS PAGE IS UNCLASSIFIED

AD-B171 686



AD \_\_\_\_\_

L  
②

BROADBAND NEAR IR LASER HAZARD FILTERS

ANNUAL REPORT

GAJENDRA SAVANT

SEPTEMBER 10, 1992



Supported by

U.S. ARMY MEDICAL RESEARCH AND DEVELOPMENT COMMAND  
Fort Detrick, Frederick, Maryland 21702-5012

Contract No. DAMD17-90-C-0086

Physical Optics Corporation  
20600 Gramercy Place, Suite 103  
Torrance, California 90501

Distribution authorized to DOD Components only, March 10, 1993. proprietary information. Other requests shall be referred to Commander, U.S. Army Medical Research and Development Command, Fort Detrick, Frederick, Maryland 21702-5012. *Attn: SGRD-RMI-S*

The findings in this report are not to be construed as an official Department of the Army position unless so designated by other authorized documents

93 3 22 026

93-05934



4988

REPORT DOCUMENTATION PAGE			Form Approved OMB No 0704-0188	
<small>Public reporting burden for this collection of information is estimated to average 1 hour per response, including the time for reviewing instructions, searching existing data sources, gathering and maintaining the data needed, and completing and reviewing the collection of information. Send comments regarding this burden estimate or any other aspect of this collection of information, including suggestions for reducing this burden, to Washington Headquarters Services, Directorate for Information Operations and Reports, 1215 Jefferson Davis Highway, Suite 1204, Arlington, VA 22202-4302, and to the Office of Management and Budget, Paperwork Reduction Project (0704-0188), Washington, DC 20503.</small>				
1. AGENCY USE ONLY (Leave blank)		2. REPORT DATE Sep. 10, 1992	3. REPORT TYPE AND DATES COVERED Annual 10 Sep 91 - 10 Sep 92	
4. TITLE AND SUBTITLE Broadband Near IR Laser Hazard Filters			5. FUNDING NUMBERS DAMD17-90-C-0086	
6. AUTHOR(S) Gajendra Savant			65502A 3P665502M802 CA DA346204	
7. PERFORMING ORGANIZATION NAME(S) AND ADDRESS(ES) Physical Optics Corporation 20600 Gramercy Place, Suite 103 Torrance, California 90501			8. PERFORMING ORGANIZATION REPORT NUMBER	
9. SPONSORING / MONITORING AGENCY NAME(S) AND ADDRESS(ES) U.S. Army Medical Research & Development Command Fort Detrick Frederick, Maryland 21702-5012			10. SPONSORING / MONITORING AGENCY REPORT NUMBER	
11. SUPPLEMENTARY NOTES				
12a. DISTRIBUTION / AVAILABILITY STATEMENT Distribution authorized to DOD Components only, proprietary information, March 10, 1993. Other requests shall be referred to the USAMRDC, ATTN: SGRD-RMI-S, Fort Detrick, Frederick, MD 21702-5012			12b. DISTRIBUTION CODE	
13. ABSTRACT (Maximum 200 words)				
14. SUBJECT TERMS RA 3; Laser; Holographic; Hazards; Filters; Passive			15. NUMBER OF PAGES	
			16. PRICE CODE	
17. SECURITY CLASSIFICATION OF REPORT Unclassified	18. SECURITY CLASSIFICATION OF THIS PAGE Unclassified	19. SECURITY CLASSIFICATION OF ABSTRACT Unclassified	20. LIMITATION OF ABSTRACT Unlimited	

## TABLE OF CONTENTS

1.0	INTRODUCTION .....	1
2.0	SUMMARY OF FIRST YEAR RESULTS.....	1
2.1	Fabrication and Processing of Broadband IR Filters .....	2
2.2	Sealing/Lamination/Encapsulation of Broad-Band IR Filters.....	7
2.2.1	Poly(vinyl Butyral) PVB as Interlayer Laminate .....	8
2.2.2	Pressure Temperature Test of Broad-Band IR Filters.....	9
2.2.3	Description of Weathering Test.....	9
2.3	Saflex Lamination Experiment .....	11
2.3.1	Testing Saflex Laminated Samples.....	12
2.3.2	Results of Temperature Stability Test.....	13
2.4	Optical Characterization of Additional BIR Filters.....	14
2.5	Photopic/Scotopic Efficiency Measurement of BIR Filters .....	21
3.0	LASER DAMAGE TESTS.....	26
3.1	Laser Pulse Characterization.....	28
3.2	Test Samples .....	30
3.3	Exposure Test Procedures .....	31
4.0	REFERENCES.....	46

DTIC QUALITY INSPECTED 1

<b>Accession For</b>	
NTIS GRA&I	<input type="checkbox"/>
DTIC TAB	<input checked="" type="checkbox"/>
Unannounced	<input type="checkbox"/>
Justification	
By	
Distribution/	
<b>Availability Codes</b>	
Dist	Avail and/or Special
E-4	

## **1.0 INTRODUCTION**

Ocular protection against laser radiation and ballistic fragments is required for military aviators and ground personnel. Protection against laser radiation in several laser hazard and threat wavelength regions is required to prevent ocular injury from existing potentially hazardous systems. The laser hazard and threat wavelengths extend from the ultraviolet through the near infrared. There is potential for a cost effective protection against fixed wavelength threats utilizing narrow-band holographic reflection filters for the visible portion of the spectrum. The IR portion of the spectrum can also be fully protected, by using the broad-band holographic filters that were being developed and tested during the first year of this program.

POC's concept of broad-band near IR reflection filter fabrication is based on volume Bragg holography using photopolymers and dichromated gelatins. The successful performance of broad-band IR filters depends upon the survivability of their optical material (in this case, photopolymer or dichromated gelatin or a modified and/or composite graft of gelatin and polymer). As a result, chemical modifications to dichromated gelatin (DCG) through synthesis and chemical wet processing, can produce DCG based broad-band filters which are very stable to environmental changes of temperature, pressure, sunlight, etc.

## **2.0 SUMMARY OF FIRST YEAR RESULTS**

During the first year of this program, POC successfully completed partial material optimization, optical adhesive evaluation, broad-band filter fabrication, and environmental testing, such as laser damage threshold and temperature stability. Encapsulation and environmental tests of selected broad-band filters are in progress. These tests will be completed next year.

In order to maintain the quality of the filter, we had planned to fabricate in the first quarter of this program, we procured high quality gelatin and ammonium dichromate. It is well known that there are several kinds of gelatins. One type of gelatin may suit one application while it may not be appropriate for other types of applications. We investigated a number of gelatin types before choosing Knox 5211 for broad-band IR filter fabrication. After choosing the gelatin and dichromate, we established the right composition of gelatin, ammonium dichromate and water. We attempted to find the optimum coating thickness for 50 nm and 90 nm bandwidth range filters.

For the production of broad-band IR filter (BIRF), POC also investigated other gelatin, photopolymers and a chemically modified (grafted) version of DCG. Compared to other holographic recording materials, DCG offers many advantages such as bandwidth, wavelength range and superior photopic/scotopic efficiency. Thus far, using DCG as a holographic recording material we produced at least an order of magnitude larger bandwidth than with Du Pont photopolymer FRS-70 or Polaroid's DMP-128. However, to accomplish successful application of DCG as a recording material for the production of BIRF, it is necessary to optimize processing steps during fabrication. These steps and parameters include:

- Select gelatin type and its bloom strength
- Determine optimum dichromate (sensitizer)/gelatin concentration ratio
- Evaluate thickness of DCG film
- Determine correct age of the film
- Outline exposure conditions such as laser wavelength, beam power, dark reaction, etc.
- Establish wet processing steps and controls
- Characterize broad-band IR reflection filters
- Establish optimum lamination/encapsulation method

## **2.1      Fabrication and Processing of Broadband IR Filters**

The basic technique for making infrared holographic mirrors is illustrated in Figure 1. A laser beam of wavelength  $\lambda_0$  is incident on a layer (typically 10-20  $\mu\text{m}$ ) of photosensitive holographic emulsion (dichromated gelatin (DCG)). The material currently in use is an advanced DCG and/or DCG-PVA graft. A laser beam passes through the holographic emulsion and is reflected by a mirror. This reflected beam now interfaces with the incoming beam to set up a standing wave pattern in the holographic emulsion. This standing wave pattern produces a set of interference fringes. Where constructive interference occurs within the material, a greater amount of energy is deposited, and where destructive interference occurs, virtually no energy is deposited. Those planes with maximum depositions of energy (constructive interference) cause changes in the index of refraction of the material, thus creating scattering planes.

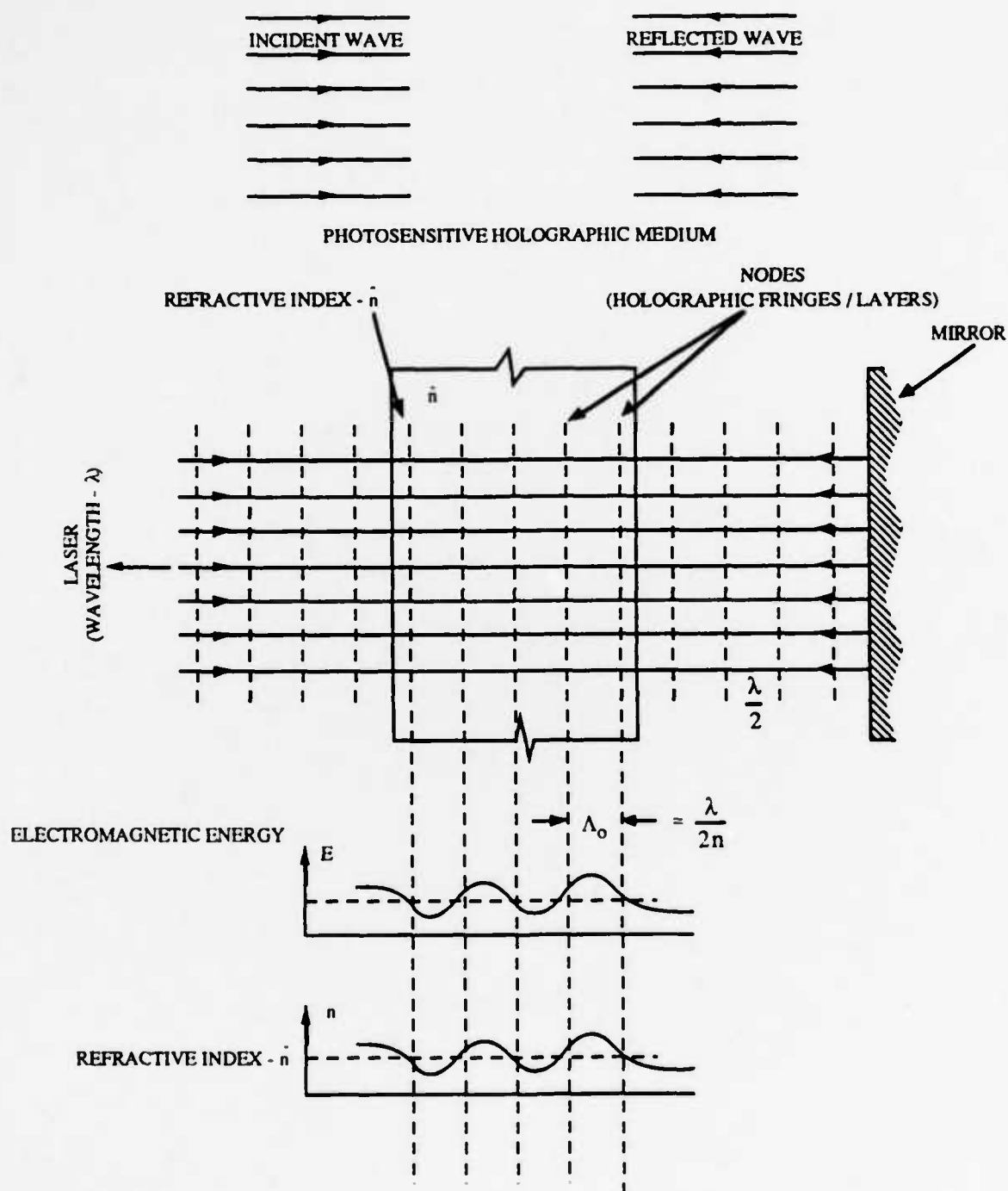


Figure 1  
Standing Wave Holographic Recording (Normal Incidence)

To understand the geometry of the holographic recording process, it is necessary to review a few principles of optics. When radiation enters a material of index of refraction  $n$ , its wavelength is reduced by a factor of  $1/n$  as follows:

$$\text{Free Space } \lambda_{v0} = C \quad (1)$$

$$\text{Medium } \lambda_{v0} = v \quad (2)$$

where  $C$  is the speed of light,  $v_0$  its frequency, and  $v$  is the velocity of radiation propagation in the medium. Now the index of refraction  $n$  is defined as:

$$n = c/v = \lambda_0 v_0 / \lambda v_0 \quad (3)$$

which yields

$$\lambda = \lambda_0 / n \quad (4)$$

showing that the wavelength in the material of index of refraction  $n$  is reduced by  $1/n$ . For standing wave patterns, the successive nodes of the standing waves occur at distances of  $\lambda/2$ . Thus, the spacing between these holographic planes,  $\Lambda_0$ , is

$$\Lambda_0 = \lambda/2 = \lambda_0/2n \quad (5)$$

To obtain an estimate of the number of holographic reflection planes in an emulsion of thickness  $20 \mu\text{m}$ , we calculate

$$\text{number of planes} = 20 \mu\text{m} / 0.5 \mu\text{m} / (2 \cdot 1.55) = 124 \quad (6)$$

Thus, for example, when recording in the visible part of the spectrum, approximately 124 holographic reflection planes can be recorded, yielding very high reflectivities (in excess of 99.9%) and OD in excess of 6, with virtually no measurable absorption in the  $20 \mu\text{m}$  layer.

In order to fabricate a broadband IR (BIR) filter, using an argon ion laser ( $\lambda = 488 \text{ nm}$  or  $514 \text{ nm}$ ), we followed two complementary methods. One method increases the angle of incidence, with a limit set by the critical angle of the air-substrate interface. The other method uses POC's proprietary wet processing technology which involves chemical/material swelling. By eliminating the interfacing problem through the use of index-matching liquid, the critical angle limit can be increased. Our holographic exposure setup is illustrated in Figures 2 and 3.



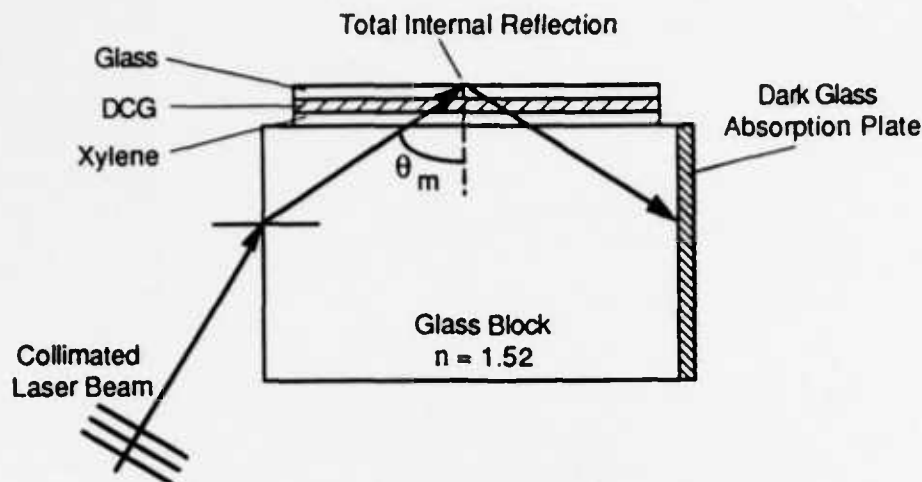


Figure 2  
Holographic Recording Setup Used to Fabricate Broadband IR Filters. Using this setup, eye protection for longer wavelengths (of up to  $2 \mu\text{m}$ ) can be accomplished.

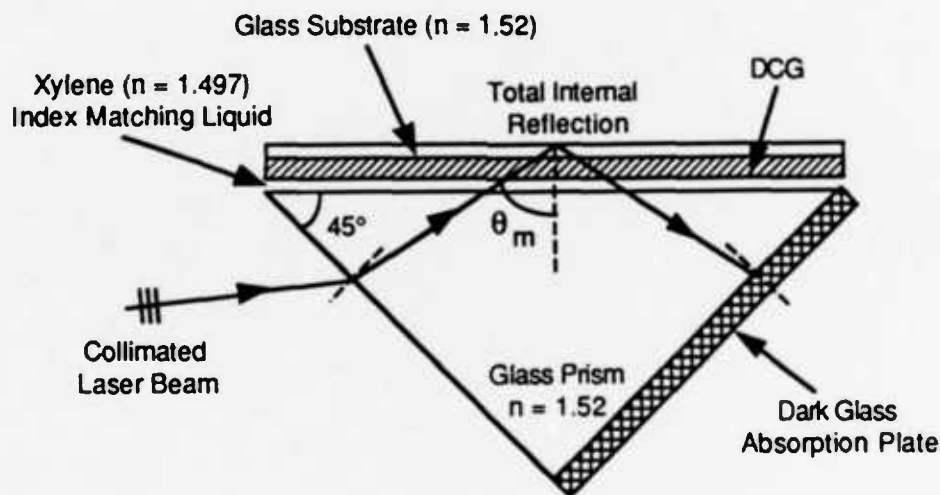


Figure 3  
Holographic Exposure Setup Used to Fabricate BIRF

These parameters are more or less interdependent, therefore, optimal thickness ( $50\text{-}100 \mu\text{m}$ ), dye-sensitizer concentration ( $0.1\text{-}1\%$ ), exposure of  $200$  to  $400 \text{ mJ/cm}^2$  and optimal processing conditions are required to achieve broadband, high optical density, and high photopic/scotopic efficiency filters. Because the filter operates in the IR region and the material is transparent in the visible spectrum, photopic/scotopic efficiencies are naturally high. An approximate angular formula for such a non-uniform Lippmann holographic filter is given by Tomasz Jansson et al. [1,2] and can be explained with the help of Figure 4.

$$\frac{\Delta\lambda'}{\lambda} = \frac{\Delta\lambda}{\lambda} + \frac{\Delta\Lambda}{\Lambda} \quad (7)$$

where

$\Delta\lambda'$  = bandwidth of the non-uniform hologram

$\lambda$  = Bragg wavelength

$\Delta\lambda$  = bandwidth for the fully-uniform case

$\Delta\Lambda$  = grating constant range

$\Lambda$  = average Bragg grating constant

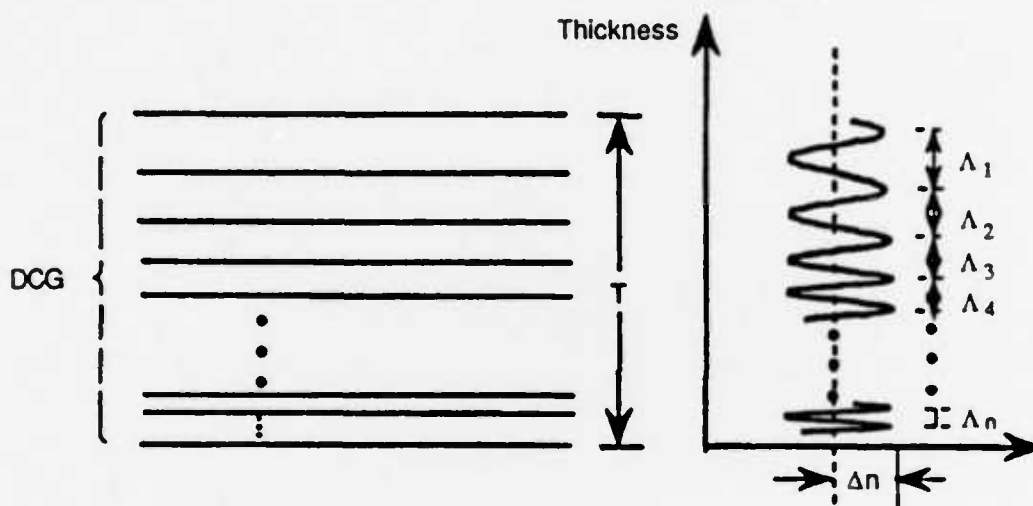


Figure 4  
Non-Uniform Bragg Planes in DCG Lippmann Holograms

The Bragg bandwidth for Kogelnik's fully uniform (high efficiency) is given by [3]

$$\frac{\Delta\lambda}{\lambda} = \frac{1}{\cos 2\phi} \frac{\Delta n}{n} \quad (8)$$

For normal incidence ( $\phi = 0$ ), Eq. (7) becomes

$$\frac{\Delta\lambda'}{\lambda} = \frac{\Delta n}{n} + \frac{\Delta\Lambda}{\Lambda} \quad (9)$$

## 2.2 Sealing/Lamination/Encapsulation of Broad-Band IR Filters

DCG or DCG based holographic recording materials are affected by high humidity, particularly when both humidity and temperature are high. The BIR filters made up of DCG also get affected by moisture, although more slowly. Therefore, BIR filters need protection either through some kind of moisture barrier, through lamination or encapsulation. The method of choice, however, depends upon the application.

During this year, we used a simple method of encapsulation by applying a transparent UV curable epoxy/adhesive and a thin glass plate. After thoroughly wet processing the BIR filter, we baked the filter at about 70-80°C for 3 hours to reduce the amount of entrapped solvent (in our case isopropyl alcohol which is used as a wet processing solvent) and moisture. The BIR filter was then cooled to room temperature. A small quantity of transparent adhesive such as Norland-63, 65 or 68, or Dymax-304, 305, or 20,000 was placed on the dry BIR filter and slowly spread using a clean thin glass plate which was then permanently placed over the epoxy/adhesive layer. When the BIR filter with a thin layer of epoxy/adhesive and a thin glass plate are exposed to UV light, the epoxy cures, bonding them together to form a single layer. Thus, the BIR filter is sandwiched between two glass plates and does not come in contact with moisture. Shrinkage of the adhesive must be minimal to ensure the stability of the filter. We are continuing to evaluate the most suitable adhesives for harsh military environmental conditions. A simple schematic of encapsulation is illustrated in Figures 5 and 6.

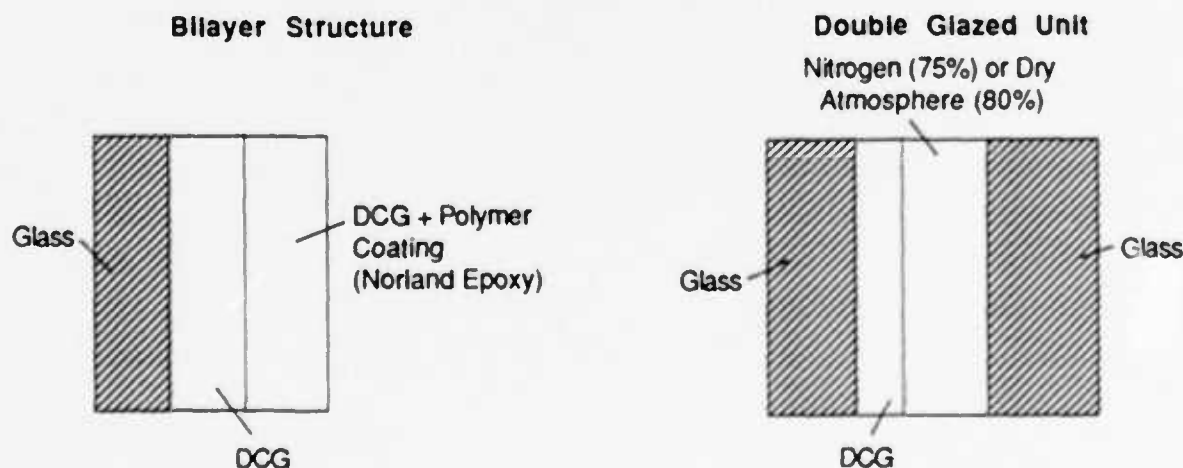
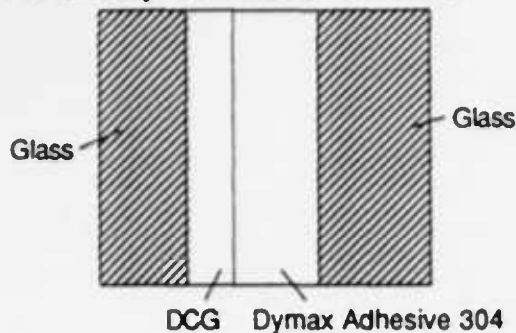


Figure 5  
Illustration of POC's Encapsulation of BIR Filters

### Preliminary Laminated Structure



### Conventional Laminated Structure

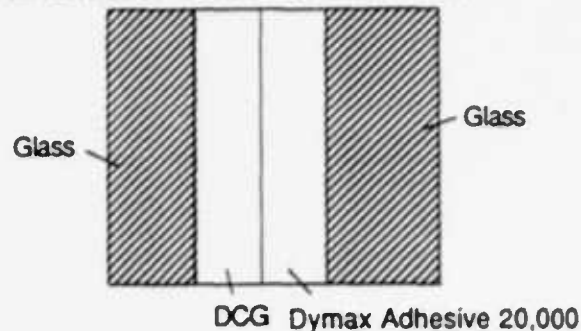


Figure 6  
Illustration of POC Encapsulation Sample Fabrication

#### 2.2.1 Poly(vinyl Butyral) PVB as Interlayer Laminate

For laminating DCG broad-band IR filters, POC used PVB purchased from Monsanto. The PVB was prepared by vacuum baking for 30 minutes at 65°C and a vacuum of 29 inch Hg, to reduce the moisture content. A cover glass was cut to size using standard 1 mm thick glass and the IR window was assembled as a unit. The assembled broad-band IR filters were positioned inside a sealed bag for the vacuum de-airing process. A minimum vacuum of 24 inch Hg was immediately drawn on the sample and was held for a minimum of 15 minutes at a ambient temperature of 22°C. With the vacuum still applied, the bag with the sample was inserted into an oven set at 88°C. The temperature as allowed to stabilize for 5 minutes and then the sample was held under 24 inch Hg vacuum for a minimum of 15 minutes. The samples were removed from the oven and care was taken not to introduce any moisture into the bags. The normally opaque PVB was now transparent and the samples were inspected for uniformly clear transparency free of bubbles, inclusions and delamination. The side view of the sample thus prepared is illustrated in Figure 7.

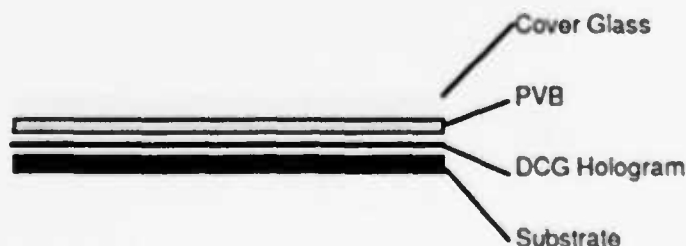
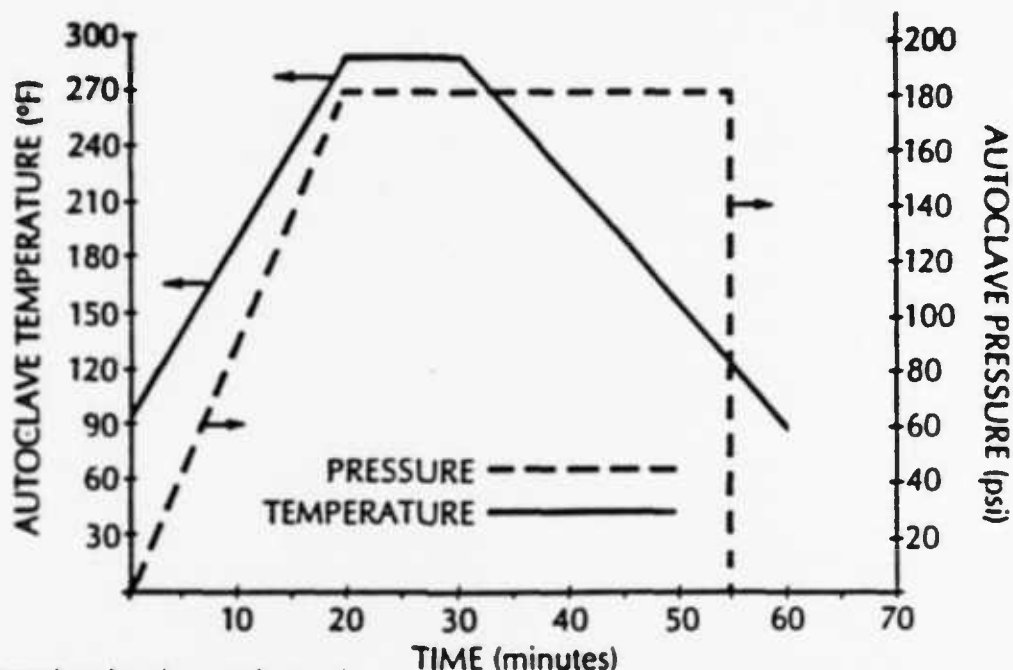


Figure 7  
Side View of Sample

### 2.2.2 Pressure Temperature Test of Broad-Band IR Filters

The autoclaving was conducted using a 100 cubic foot autoclave which was rented on site at Thermal Equipment Company, Torrance, California. The autoclave cycle was conducted as shown in Figure 8.



The data set forth in this graph are based on samples tested and are not guaranteed for all samples or applications. The data are intended as guides and do not reflect product specifications for any particular property.

Figure 8  
Autoclave Cycle

Dry nitrogen was used to pressurize the autoclave. After completion of the autoclave cycle, the samples were vacuum baked for a minimum of 8 hours at 29 inch Hg and at 65°C. The samples were removed from the oven and the edges were sealed immediately with Norland 61 UV curing adhesive.

### 2.2.3 Description of Weathering Test

The laminated glass samples were exposed to a weathering test in accordance with ANSI Z26.1 Section 5.16 which subsequently references ASTM G23.

The twin carbon arc apparatus operates on a two hour cycle which exposes the panel to light without water spray for 102 minutes and light with water spray for 18 minutes. The machine operates approximately 20 hours per day, 5 days per week.

The average voltage and amperage for each trim period are 135 volts and 16 amperes (alternating current). A black panel temperature of  $145^{\circ}\text{F} \pm 5^{\circ}\text{F}$  is maintained. Water strikes the sample in the form of a fine spray under a pressure of 25-30 psi, a pH of 6.0 to 8.0 and has a temperature of  $60^{\circ}\text{F} \pm 10^{\circ}\text{F}$ . A comparison of spectral distribution for actual sunlight to the light emitted by the carbon arc machine is illustrated in Figure 9(a). A typical sample curves are illustrated in Figures 9(b) and 9(c). The curves shows the stability of POC's samples.

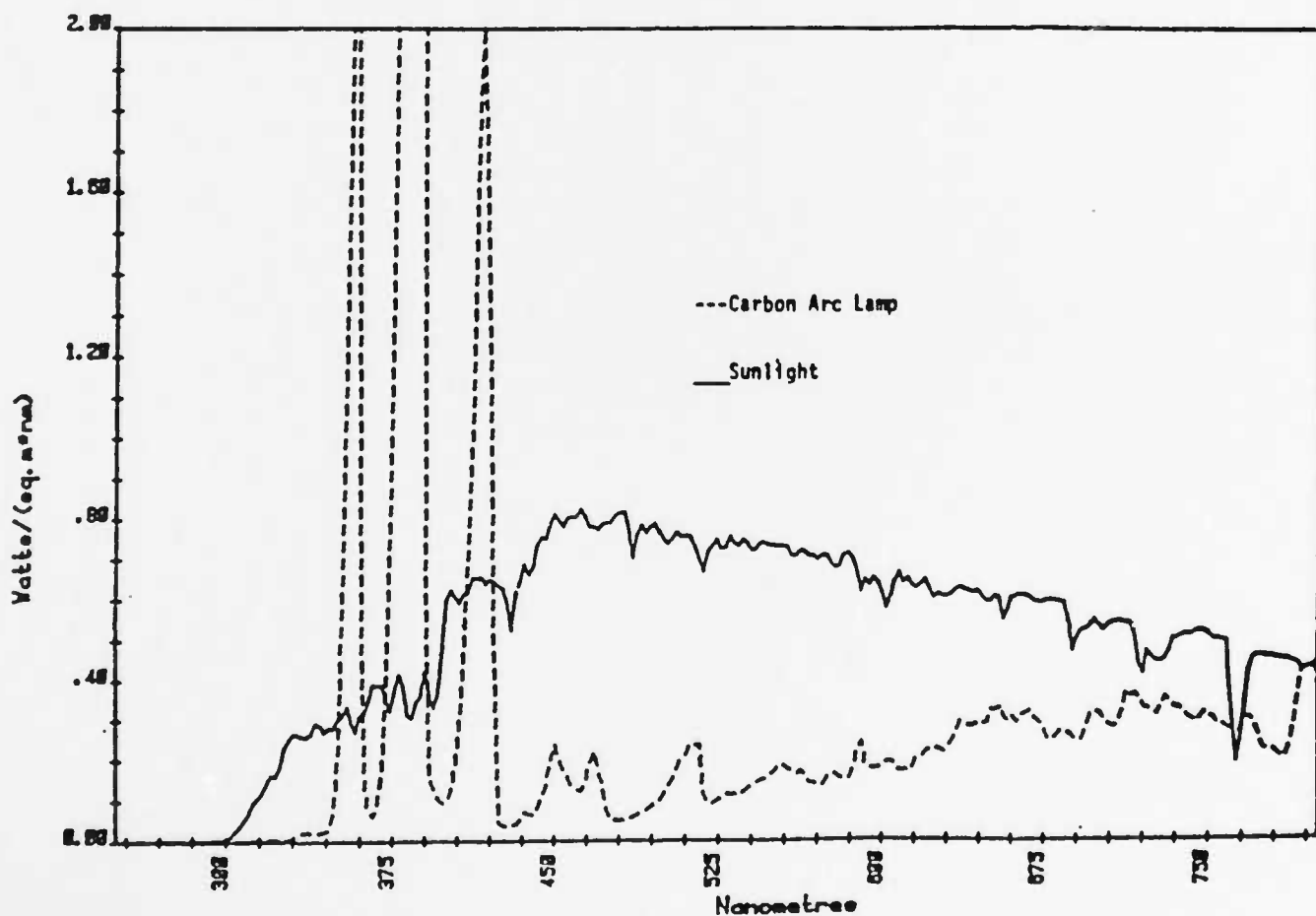


Figure 9(a)  
Atlas Electric Devices; Spectral Power Distribution; Atlas Enclosed Violet Carbon Arc Lamp

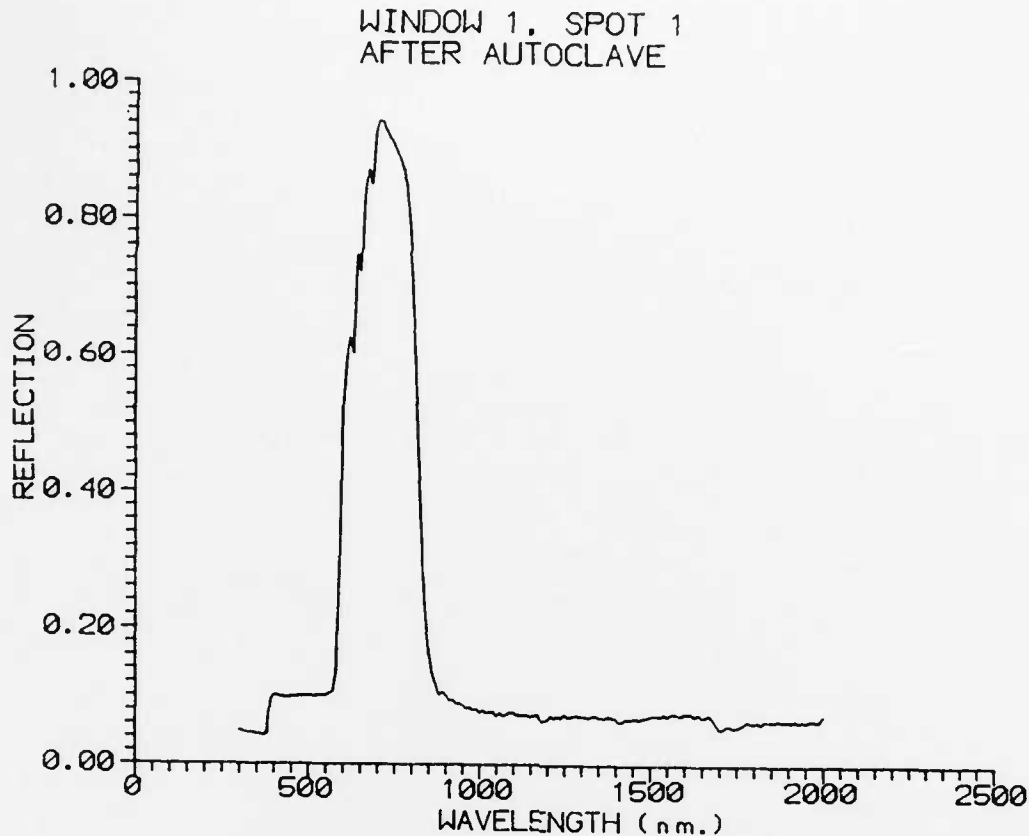


Figure 9(b)  
Reflectivity Curve of a Typical Broadband Sample Immediately After Removing from the Autoclave

### 2.3 Saflex Lamination Experiment

During the early trial stages of laminating DCG based infrared films with Saflex it was discovered that combining DCG with Saflex caused the bandwidth to shift an average of 200 nm into the blue with a 160 nm reduction in the bandwidth. Although it has been known that a combination of temperature and pressure resulted in blue shifting and bandwidth reduction, never had the effect been demonstrated to be so dramatic. It was apparent that the Saflex material was adversely effecting the DCG based infrared films. It was surmised that a possible candidate for the cause of degradation was the residual 0.3 - 0.4% water content of the Saflex film. In an effort to prove our assumption the following experiment was conducted.

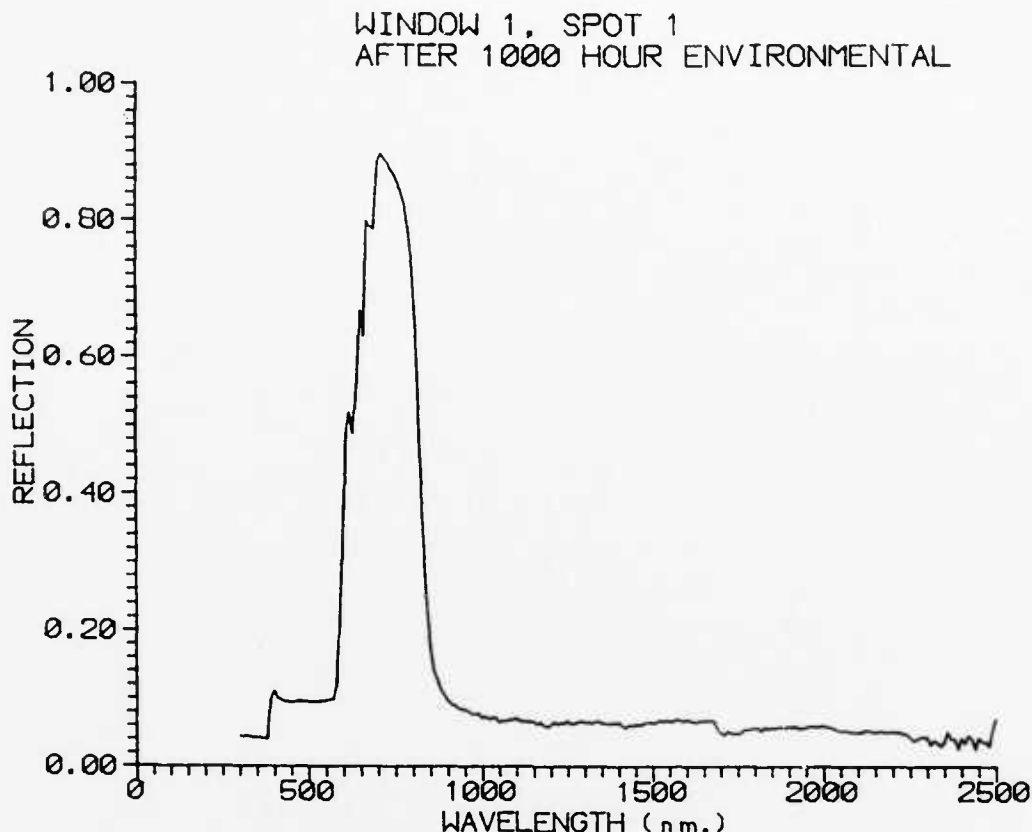


Figure 9(c)  
Reflectivity Curve of a Typical Sample After Keeping the Sample in Autoclave for 1000 hours

### 2.3.1 Testing Saflex Laminated Samples

The unlaminated 8" x 10" samples were cut into 2" x 2" squares. The edges of the 2" x 2" squares were edge scribed the standard 1/4" from the perimeter thus making an effective clear aperture of 1 3/4" x 1 3/4". The sample group of 20 units was divided into two subgroups of 10 pieces each.

The first group of 10 pieces were placed in a Class 100 clean oven set at 120°C for 2 hours. The samples were configured on a raised mounting rack to ensure that they were not thermocoupled to the oven wall. After completion of the bake cycle the samples were then taken out of the oven one by one, optical measurements were conducted using the Perkin Elmer Lambda 9 spectrophotometer before and after lamination with the Saflex PVB. The samples were stored in a nitrogen purged dry box prior to the autoclave cycle.



The second group of 10 pieces were laminated with Saflex, aged to various dryness levels per the following schedule:

Quantity	Procedure
2	Untreated
2	Vacuum Baked @ 65°C for 10 minutes
2	Vacuum Baked @ 65°C for 30 minutes
2	Vacuum Baked @ 65°C for 60 minutes
2	Vacuum Baked @ 65°C for 90 minutes

All the samples in Group I and II were autoclaved together during the same autoclave cycle. The transmission spectrum of all the samples were collected for comparison.

### 2.3.2 Results of Temperature Stability Test

The results of the experiment are shown in Figures 10 and 11. It is clearly apparent that a PVB bake of 60 minutes at 120°C minimizes the peak wavelength shift (105 nm) and the overall bandwidth loss (50 nm). The actual performance data (see Table 1) illustrated that the average peak wavelength shift was held to an average of 61 nm with the average bandwidth shrinkage of 41 nm for the test samples.

This effect can easily be compensated for by purposely recording the IR window red shifted 60 nm and expanding the bandwidth appropriately to compensate for the shrinkage. In fact POC has experimentally fabricated broadband IR mirrors with 400 nm bandwidth (see Figure 12) with no trace of a visible second harmonic and has produced broadband IR mirrors with 550 nm bandwidth (see Figure 13) with a visible second harmonic which will be illuminated in the next several months.

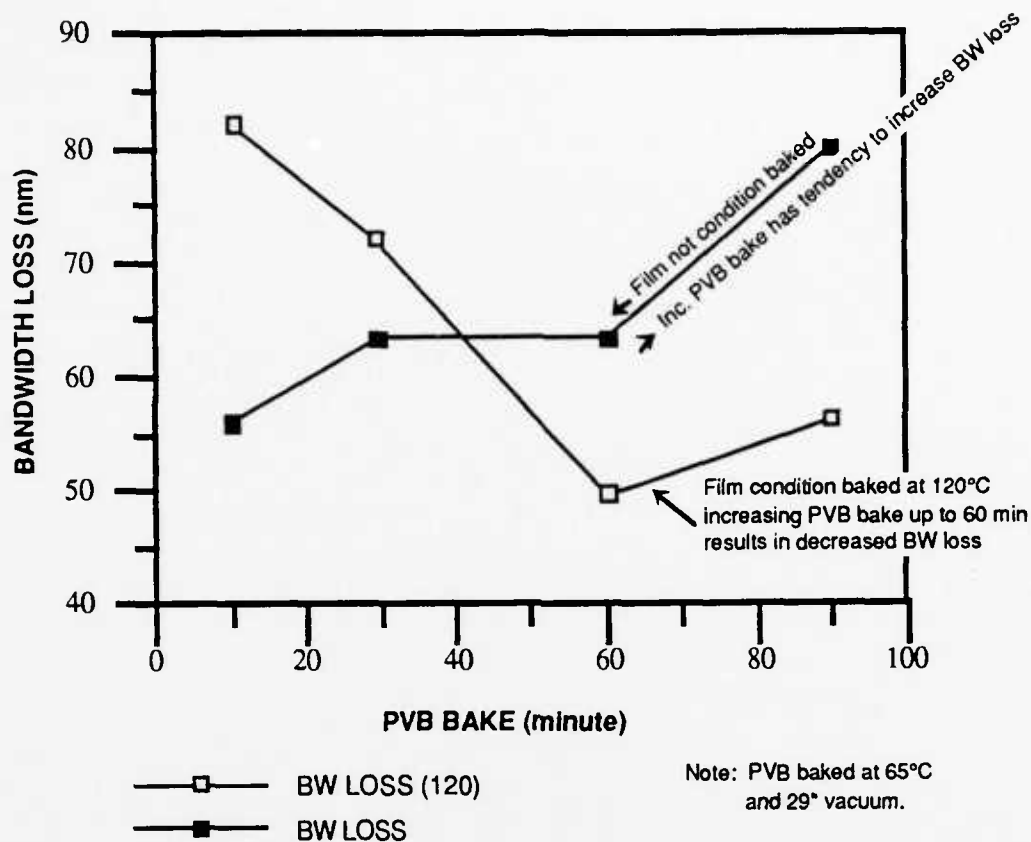


Figure 10  
PVB versus B.W. Loss

## 2.4 Optical Characterization of Additional BIR Filters

As process optimization efforts continue, we have fabricated and characterized a series of samples of BIR filters. The filters were characterized both before and after encapsulation. The characterization included:

- Bandwidth
- Transmission
- Optical density
- Peak wavelength
- Reflectivity
- Haze
- Diffraction efficiency and uniformity
- Prismatic deviation

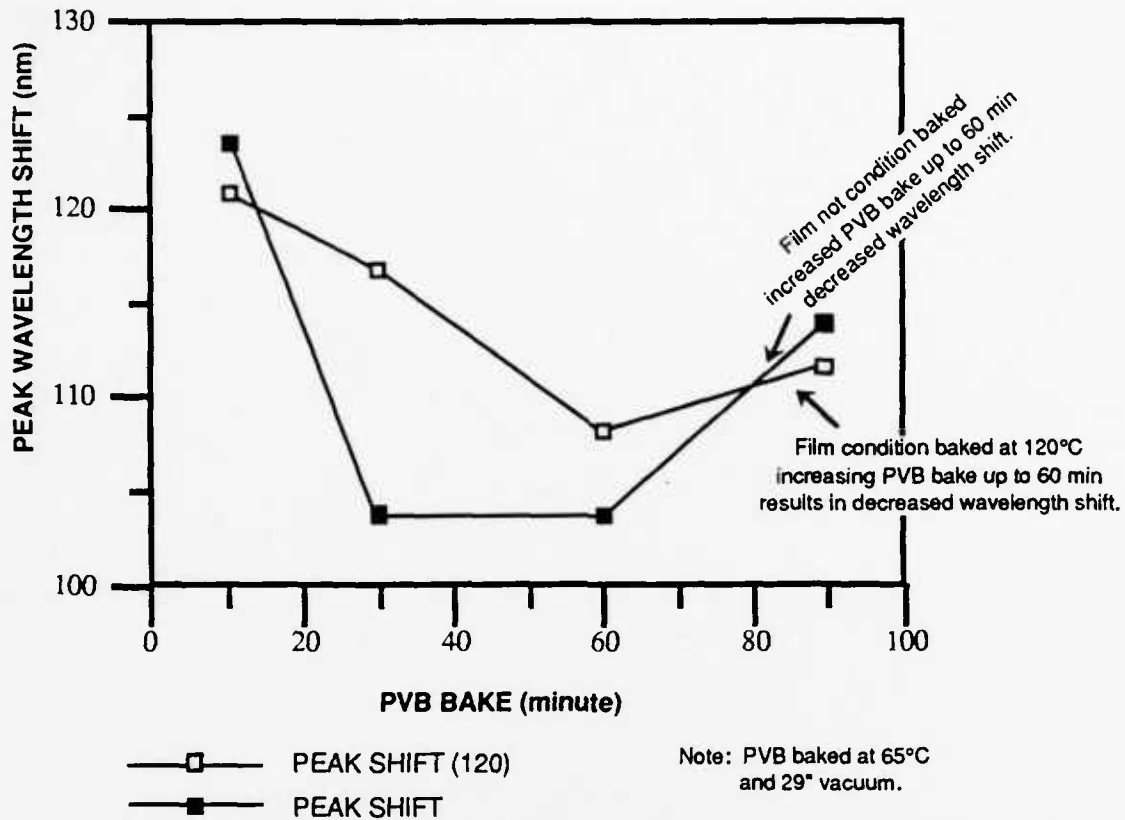


Figure 11  
PVB versus Wavelength Shift

Table 1. Description of PVB Laminated Sample Parameters

Sample	Bandwidth BL (nm)	Bandwidth AL (nm)	$\lambda$ Shift (nm)	Bandwidth Shrinkage (nm)
1 Spot 1	265	230	63	35
Spot 2	275	230	58	45
Spot 3	275	235	65	40
5 Spot 1	240	200	60	40
Spot 2	250	220	45	30
Spot 3	245	220	53	25
6 Spot 1	270	225	58	45
Spot 2	275	230	63	45
Spot 3	295	230	83	65

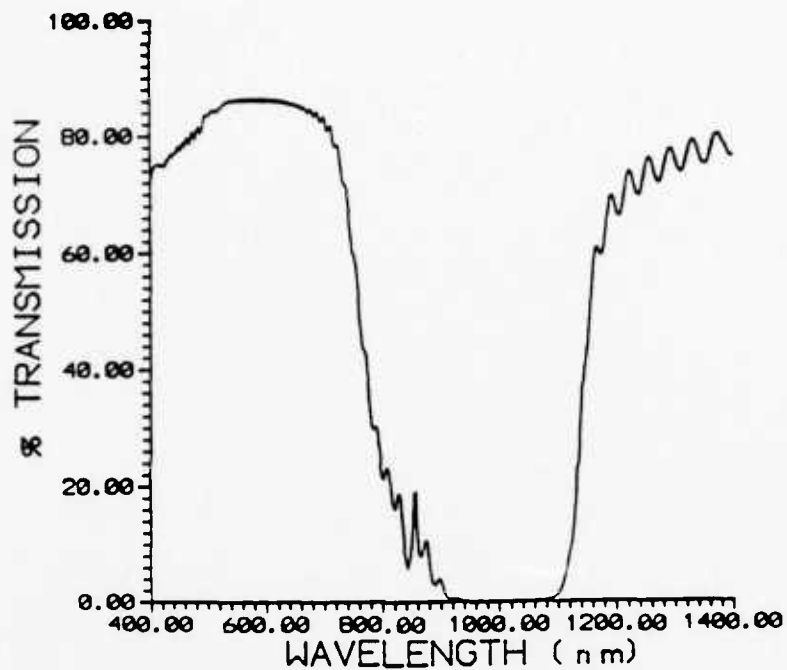


Figure 12  
400 nm Bandwidth

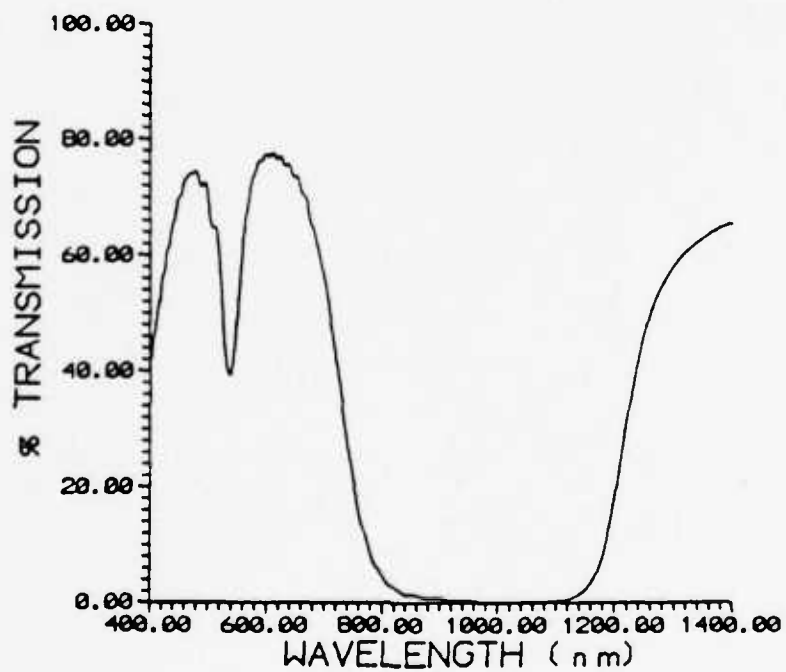


Figure 13  
550 nm Bandwidth

One of the problems we experience in fabricating high optical density broadband IR filters, is the generation of a second harmonic peak at location half the peak wavelength of IR broadband peak. Currently, we are working towards reducing the magnitude of the second harmonic peak.

The UV-visible-IR spectra of all the samples were recorded using the Perkin Elmer Lambda 9 spectrophotometer. The spectrophotometer is equipped with a common beam depolarizer and an integrating sphere detector. The use of the integrating sphere detector allows transmission and reflectivity of each sample to be recorded. Labsphere SRS-99 white standards were used as 100% reflecting standards.

The spectrophotometer is controlled by an IBM PS/386 computer operating SCAN9 software, purchased from Softways, Inc.

For transmission measurements, the BIRF samples were placed in the compartment normally used for sample cells, in front of the exit window. Since the optical path from the sample to the integrating sphere is long, any scattered radiation (haze) will not reach the integrating sphere. The reflectivity is measured by placing the sample at the sample port of the sphere and backing the sample with a black rubber cone and a graphite plate, to prevent transmitted light from re-entering the sphere. In all cases, for both transmission and reflectivity measurements, the light was incident on the BIRF first (for un laminated samples) or the glass plate on which the hologram was coated (for laminated samples).

To measure the transmission spectra at 30 and 60 degrees incidence (measured from the surface normal), a sample holder with slots machined for 30 and 60 degree incidence was placed in front of the sphere entrance port and the samples placed in the holder. To obtain reflectivity spectra at 30 and 60 degrees, the BIRF were placed in the variable angle reflectance (VAR) accessory made by Perkin Elmer for the Lambda 9.

The variability in the bandwidth of IR Lippmann structures results from shifts in the position of the low energy edge of the peak. The high energy edge tends to be more stable in position. The location of the primary peak, along with its bandwidth directly determines the location, shape and intensity of the second harmonic peak. As shown in Figure 14, the larger the primary bandwidth, the more pronounced the second harmonic. It is necessary to reduce the intensity of the second harmonic peak to as low a figure as possible to achieve neutral tint in both transmission and reflection. The primary cause of the variation in the position of the low energy band edge and the intensity of the second harmonic peak can be determined from theoretical considerations. Changes

in the functional form of the refractive index with position and/or a change in the thickness of the layers with respect to position will lead to these anomalies. It is well known that if the refractive index varies sinusoidally with position, only the first order reflection will appear; thus the appearance of higher order peaks implies that the refractive index variation is no longer purely sinusoidal but more like a square-wave character. One way to accomplish this is to over-expose the film during the wet processing. A typical exposure curve for a photosensitive film shows that the amount of photochemical change in the film increases slower than linearly in the over exposure region creating profile closer to the square wave. Careful control of the degree of exposure is necessary to obtain the desired profile. Lack of control is responsible for the variations in the second harmonic peak intensity. Figures 15(a) through 15(c) show the measured transmission and optical density of POC's BIR filters over the visible and near IR spectrums.

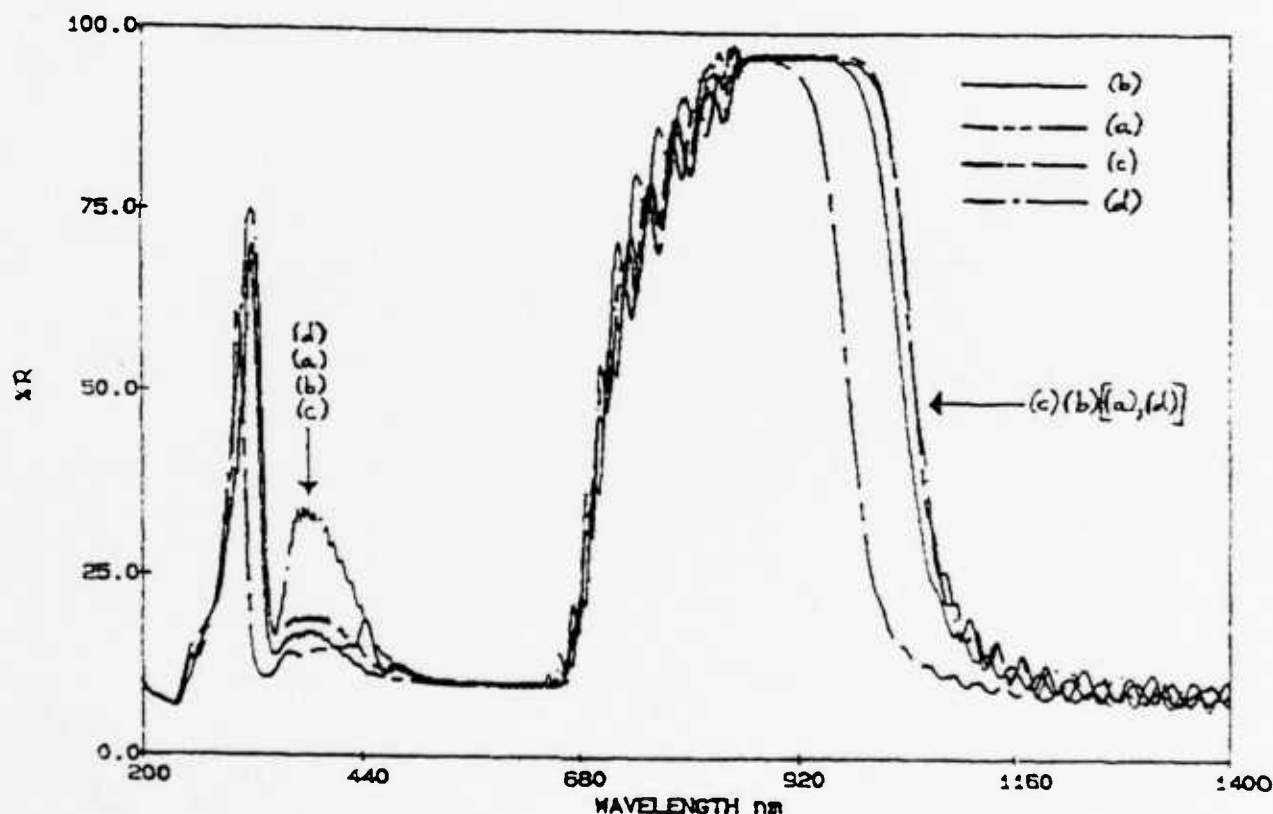


Figure 14  
Illustration of POC's Broadband IR Filters with Reduced Second Harmonic

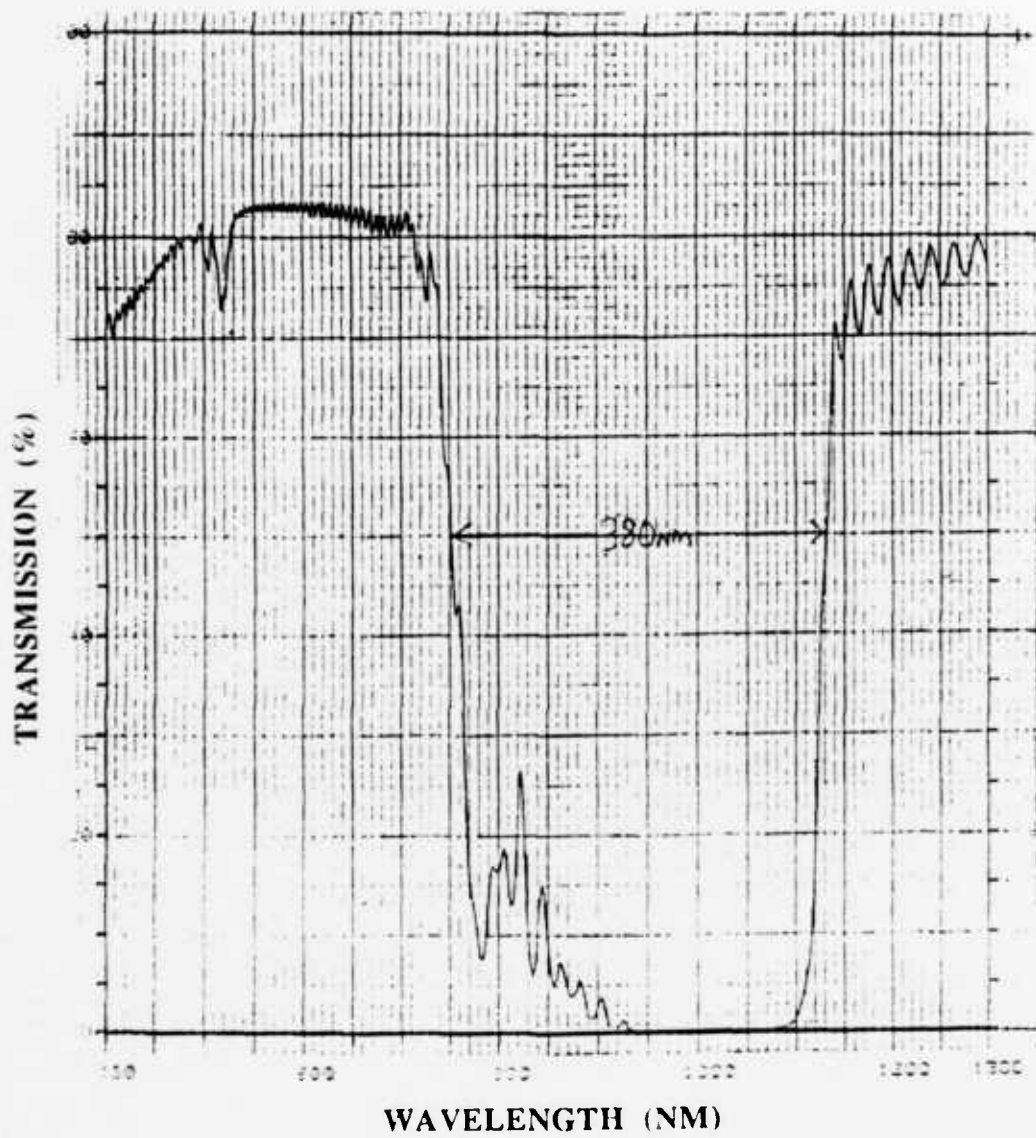


Figure 15(a)

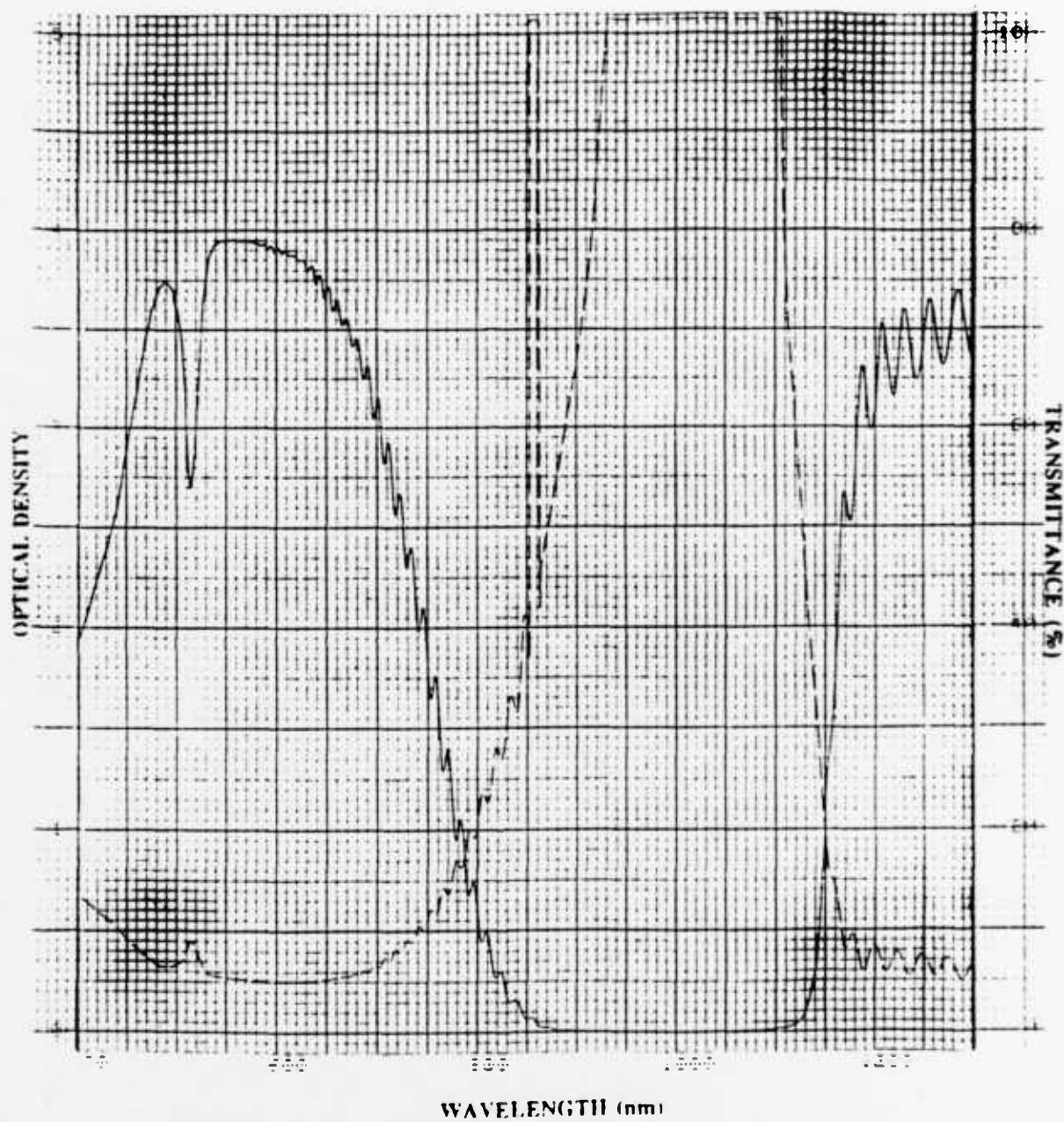
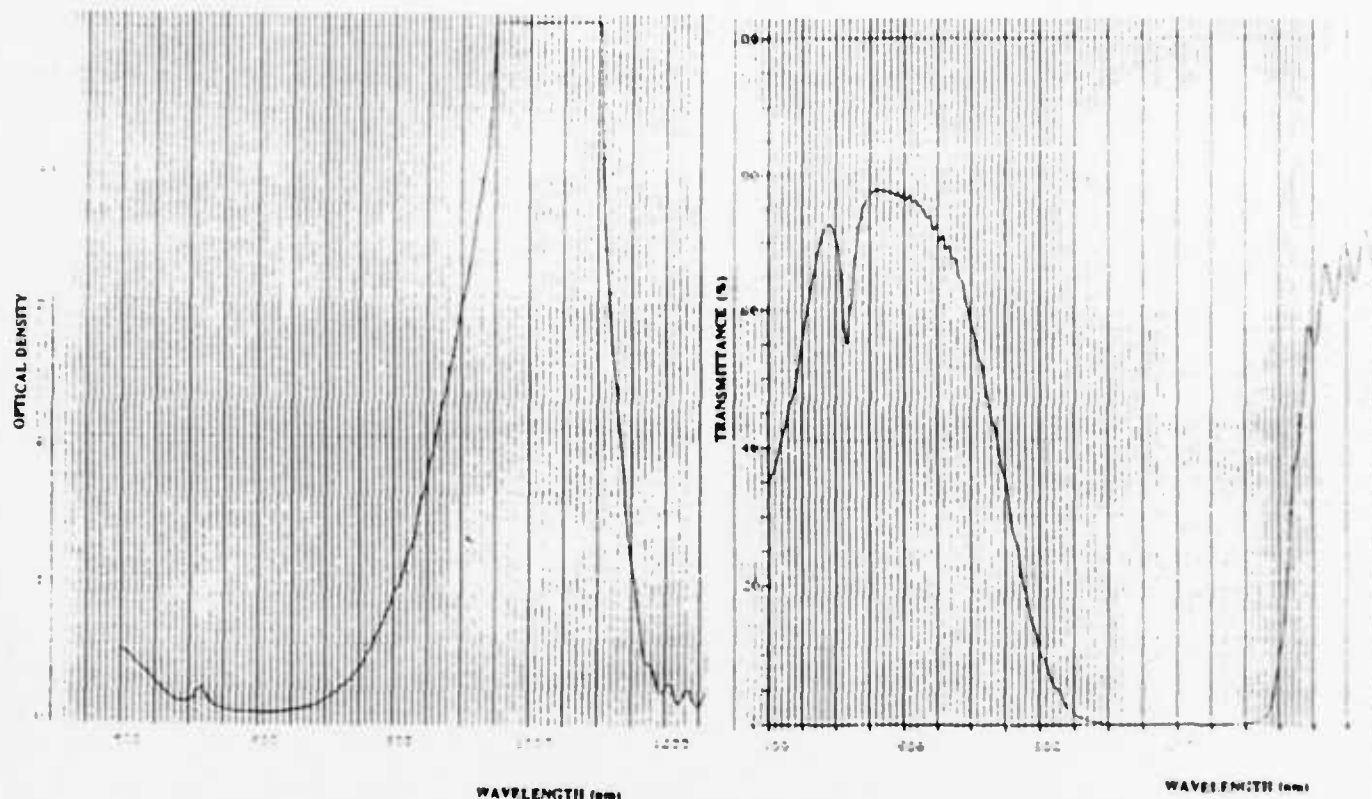


Figure 15(b)





(c)

Figure 15  
Illustration of Typical BIRF with Improved Reduction of the Second Harmonic

## 2.5 Photopic/Scotopic Efficiency Measurement of BIR Filters

Our standard broadband chirped Lippmann process modified to achieve a steep antistokes slope profile was utilized. Chirp was attained by underexposure and overmodulation during wet processing. A steep antistokes slope profile is required for optimum photopic efficiency (see Table 2).

By using the chirping method, bandwidths of  $\geq 50$  nm and  $\geq 90$  nm were attained. Photopic and scotopic efficiencies of  $\geq 80\%$  were easily achieved. The filters were relatively free of second harmonics as the location of the second harmonic is located at the UV/visible boundary.

Table 2. Optical Characteristics and Scotopic/Photopic Efficiency of POC BIR Filter

	Bandwidth (nm)	Peak Wavelength (nm)	Photopic (%)	Scotopic (%)
BIR-1	53	775	83.5	85.9
BIR-3	48	785	86.3	86.6
BIR-2	96	818	81.9	83.6
BIR-4	90	820	82.5	81.6

A second set of samples with center wavelengths at 940 nm, 890 nm and 840 nm with an achievable bandwidth of 75 nm were fabricated (data enclosed). In this case, it was demonstrated that the difficulty in suppressing the second harmonic (now moved to the visible region) partially offsets the benefits of the larger achievable bandwidths.

It is understood that optimization of photopic efficiency is dependent on the absence of second harmonics in the visible region along with a very steep antistokes slope.

As a result of POC's commercial Raman filter line experience, substantial improvements in this area have been demonstrated.

The actual spectral curves for which photopic/scotopic efficiency of selected BIR filter is measured are illustrated in Figure 16 through 19.

# BIR-1

Datfile = DC881  
Incident Angle (Degree) from Air = 0  
% Photopic TV = 83.4753  
% Scotopic TV1 = 85.8909  
End of Computation

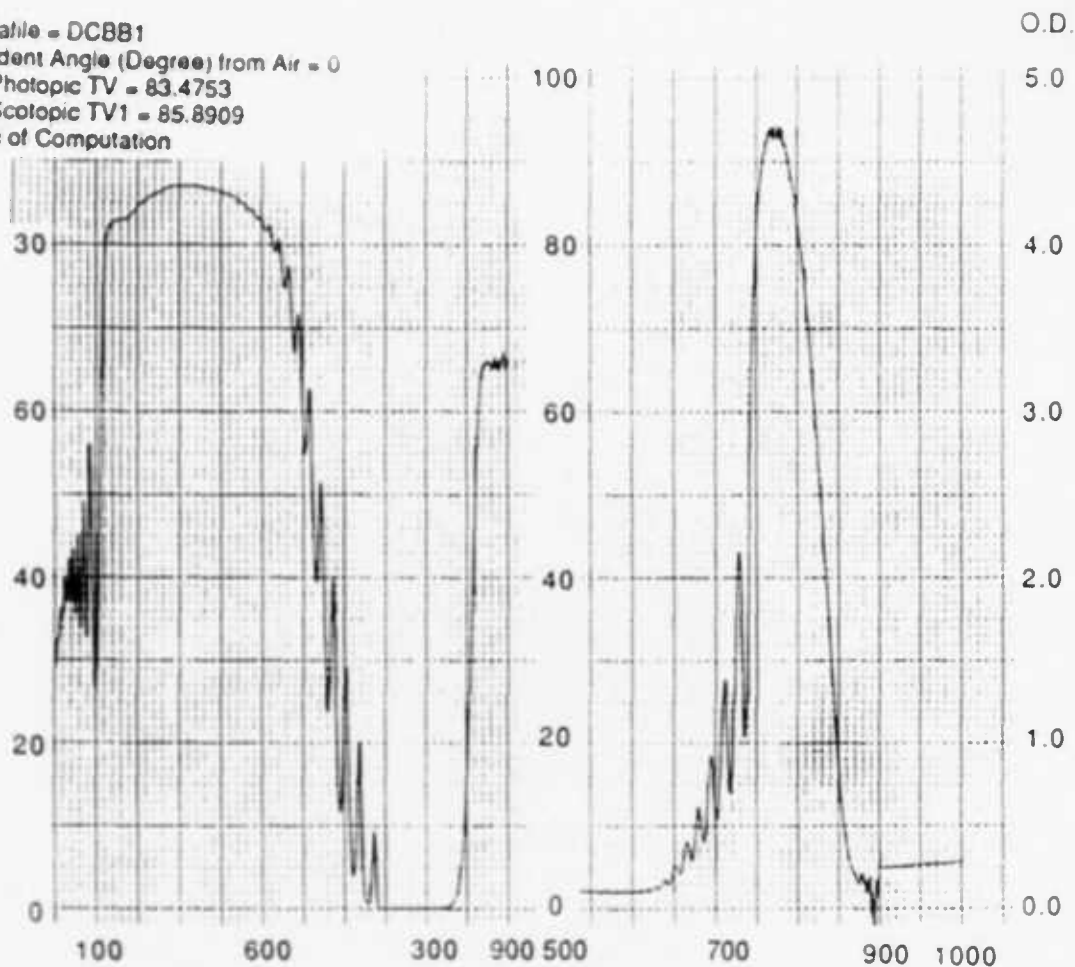


Figure 16  
POC's Broadband IR Filter Recently Fabricated in POC's Laboratory.  $\Delta\lambda = 53$

# BIR-2

Datafile = DCBB2  
Incident Angle (Degree) from Air = 0  
% Photopic TV = 81.9213  
% Scotopic TV1 = 83.6078  
End of Computation

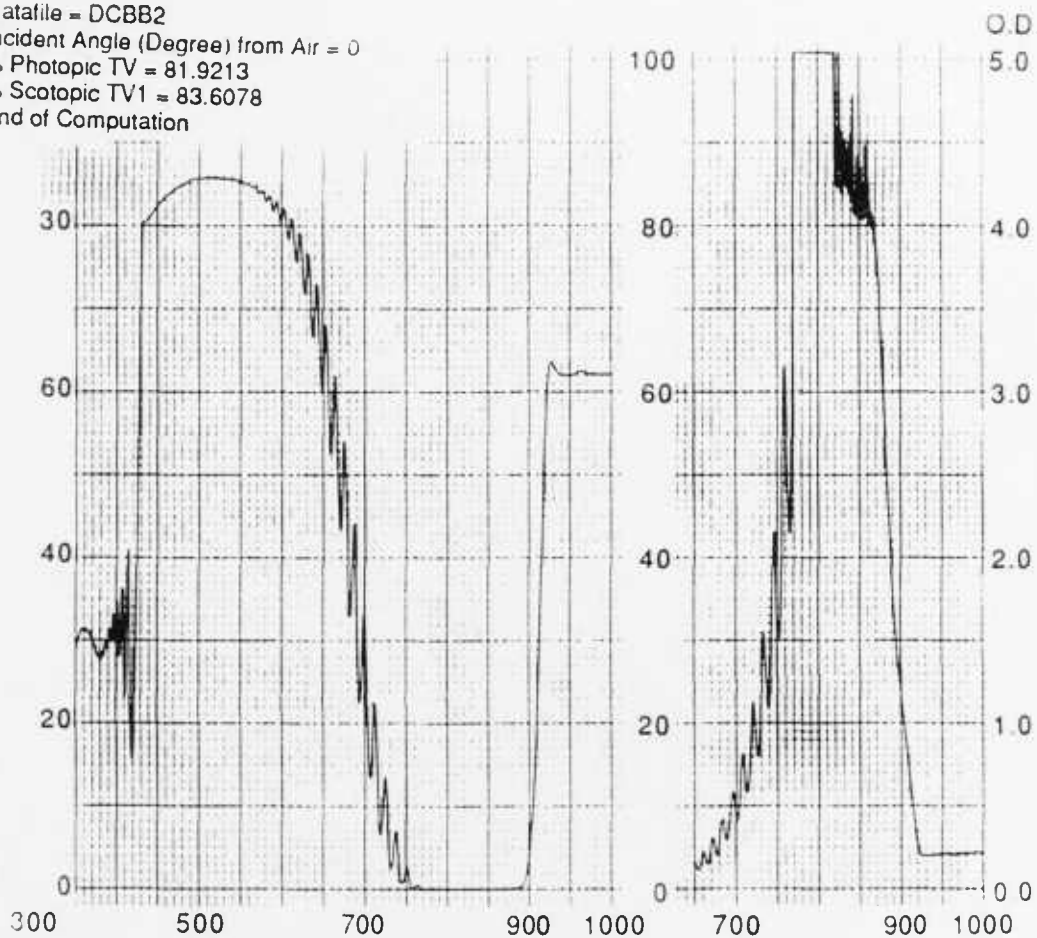


Figure 17  
POC's Broadband IR Filter Fabricated in this Quarter of Phase II.  $\Delta\lambda = 96$

# BIR-3

Datfile = DCBB3

Incident Angle (Degree) from Air = 0

% Photopic TV = 86.2551

% Scotopic TV1 = 86.6201

End of Computation

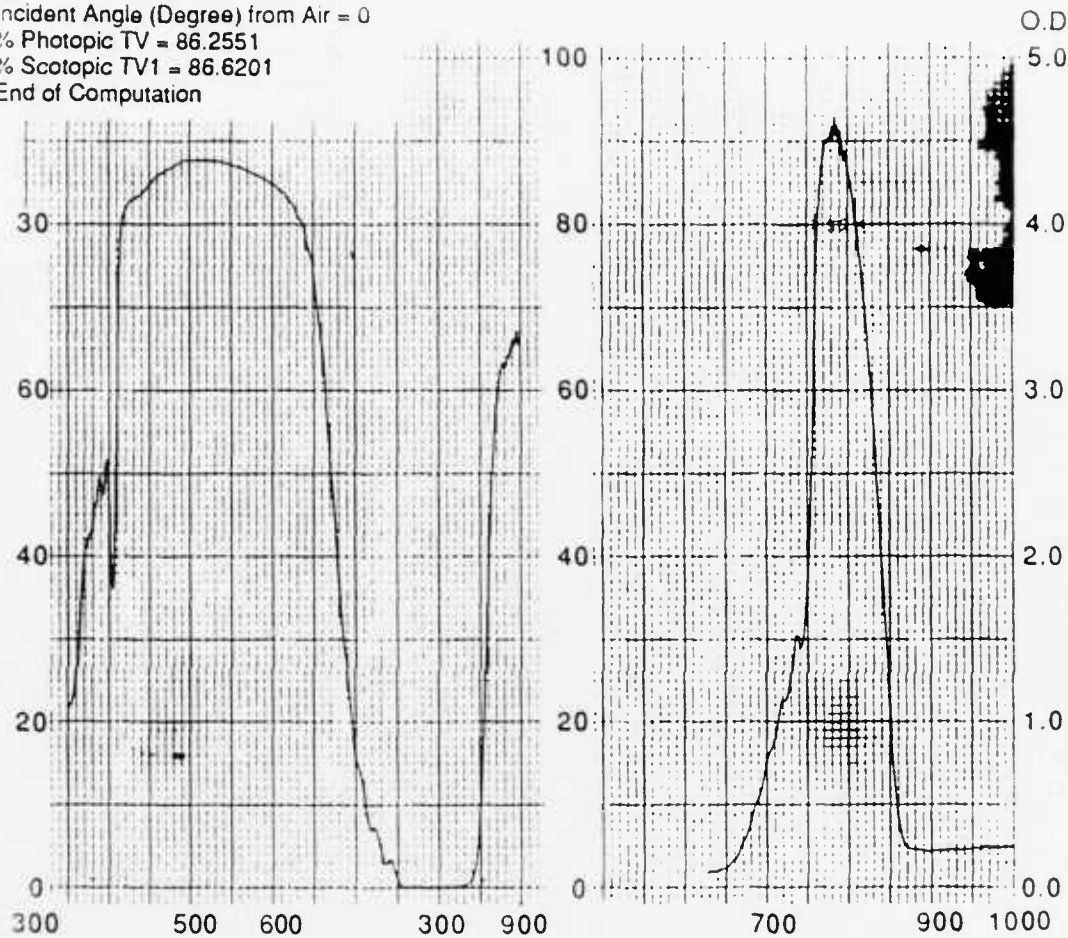


Figure 18  
POC's Broadband IR Filter Fabricated in this First Quarter of Phase II.  $\Delta\lambda = 48$

# BIR-4

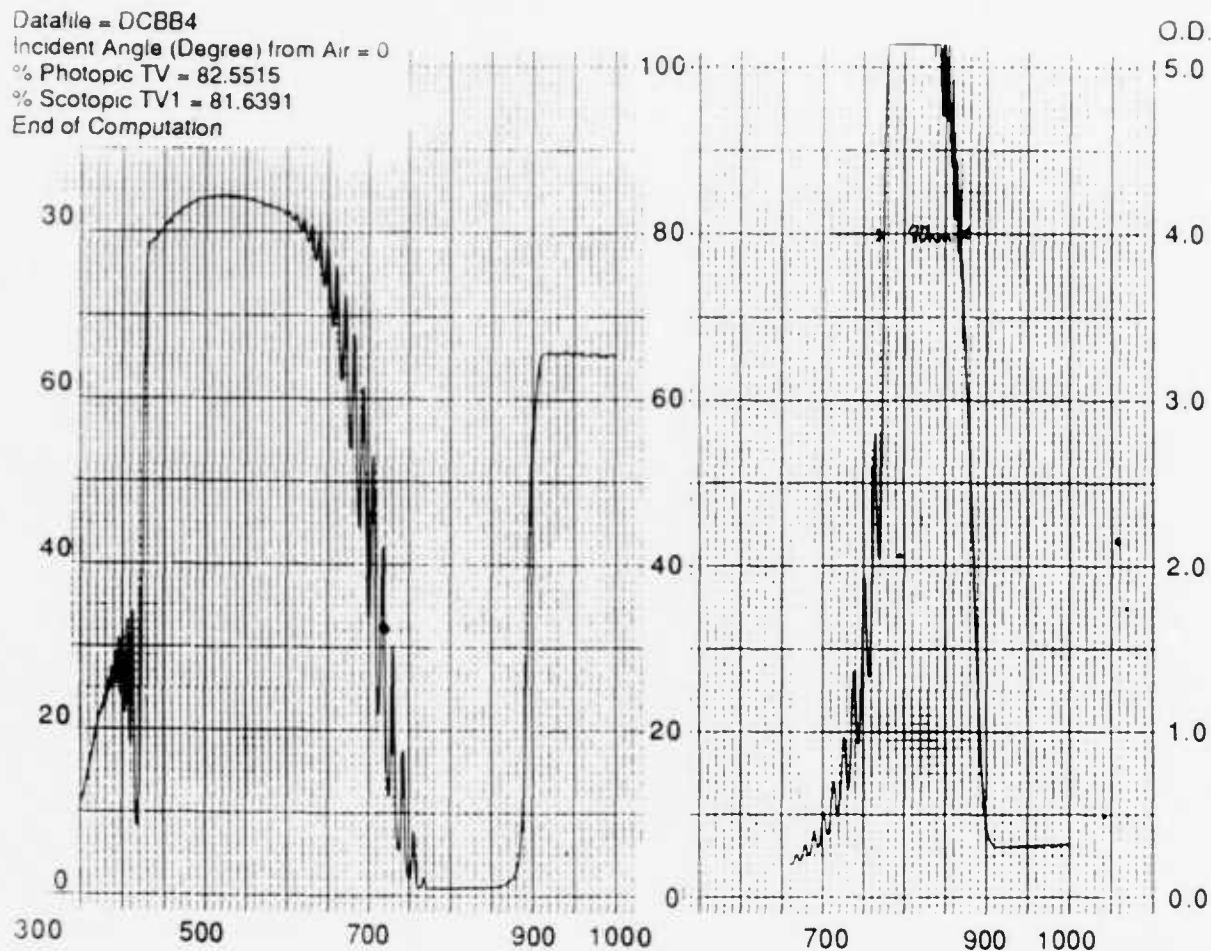


Figure 19  
POC's Broadband IR Filter Fabricated in this Quarter of Phase II.  $\Delta\lambda = 90$

## 3.0 LASER DAMAGE TESTS

POC's selected broad-band IR filters were tested for laser damage by Montana Laser Optics, Inc. A representative exposure test arrangement is shown in Figure 20, and pertinent parameters for two Nd:YAG test stations are summarized in Tables 3 and 4. The test sources are flashlamp-pumped, electro-optically Q-switched, Nd:YAG oscillator-amplifiers constrained to operate in a

single transverse mode ( $TEM_{00}$ ) using an intracavity aperture. The three-color station has frequency doubling and tripling crystals. It uses a thin intracavity etalon to limit the number of longitudinal modes, resulting in a smooth temporal waveform (with approximately 5% high frequency amplitude modulation superimposed on it). Pulse width is set to the required value by altering Q-switch timing, laser resonator length, or both.

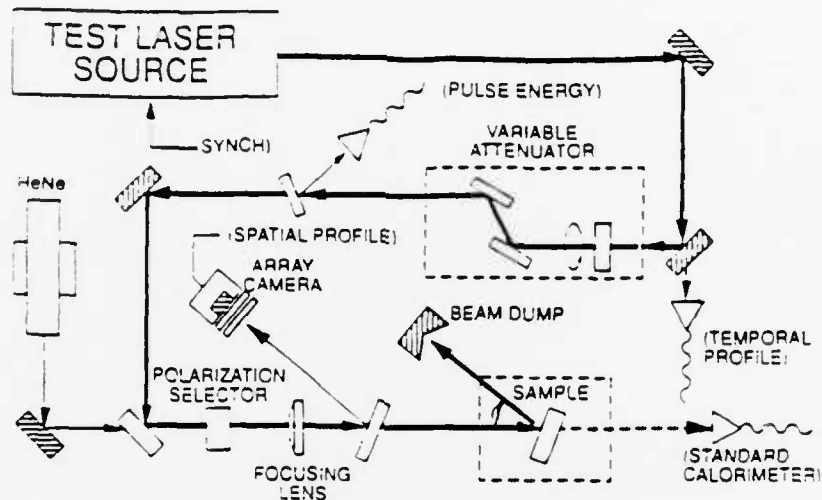


Figure 20  
Production (20/20) Nd:YAG Test Station Layout (See Text for Description)

Table 3. 3-Color Nd:YAG Test Station Specifications

Wavelength:	1064 nm-532 nm-355 nm
Pulse Energy:	750 mJ-300 mJ-100 mJ
Repetition Rate:	Up to 20 Hz, in discrete steps
Temporal Profile:	Etalon-smoothed waveform
Pulse Duration:	10-35 ns, FWHM
Spatial Profile:	$TEM_{00}$
Spot Size:	Up to 8 mm, $FW1/e^2$
Incidence Angle:	Normal to grazing
Polarization State:	Linear or circular

Table 4. Production (20/20) Nd:YAG Test Station Specifications

Wavelength:	1064 nm
Pulse Energy:	100 mJ
Repetition Rate:	Up to 20 Hz in discrete steps
Temporal Profile:	Single maximum
Pulse Duration:	20 ns
Spatial Profile:	TEM <sub>00</sub>
Spot Size:	0.5, 1, 1.5, 2 mm
Incidence Angle:	Normal to grazing
Polarization State:	Linear or circular
Exposure Sequence:	Fully programmable

The output of a test source is set to the desired level with a variable attenuator, combined at a dichroic with the visible beam from a helium-neon laser (HeNe), and delivered to the test sample located at or behind the focus of a best form positive lens. Use of a lens permits destructive energy densities (fluences) to be generated at the test sample. The lens is mounted on a translation carriage which allows the irradiated spot size to be set to the desired value; once set, the spot size is held constant during the test. The sample is mounted in a precision multi-axis manipulator which is used to position different test sites in the beam and to set the incidence angle. The polarization state is selected with a waveplate. The incident laser pulse is sampled with uncoated quartz wedges; portions of the beam are directed to various detectors for measurement of total pulse energy, spatial profile and temporal waveform. The sample surface and the visible laser radiation scattered from it are observed with a 20X optical microscope (not shown).

### 3.1 Laser Pulse Characterization

Damage test results are usually reported in terms of maximum (peak) fluence ( $\text{J}/\text{cm}^2$ ). The parameter routinely varied in an exposure test, however, is the total pulse energy (J), since this can be done easily and accurately by adjusting the attenuator and measuring energy per pulse incident at the sample under test. Evaluation of the energy distribution in space (spatial profile) and time (temporal profile) is more complex and is performed periodically. Rigorous relationships between pulse intensity, fluence, and energy follow from integration of the pulse profiles.



Absolute single-point calibration of the energy monitoring system is performed by removing the sample and allowing the laser pulse to enter a calibrated volume-absorbing disk calorimeter directly. The calorimeter is a commercial device with manufacturer's stated accuracy. Periodic calibration verification is performed by direct comparison to a second calorimeter and in accordance with MIL-C-45662A.

The temporal profile is observed with a fast silicon photodiode and calibrated 400 MHz oscilloscope. A typical Q-switched pulse waveform is shown in Figure 21. The shape is nearly Gaussian, but with an extended tail which contains a non-negligible fraction of the pulse energy. Numerical integration of this waveform yields the ratio of total pulse energy to pulse peak power. This ratio is called the effective pulse width. The photodiode is also used to monitor shot-to-shot variation in the temporal profile which is typically less than 5%.

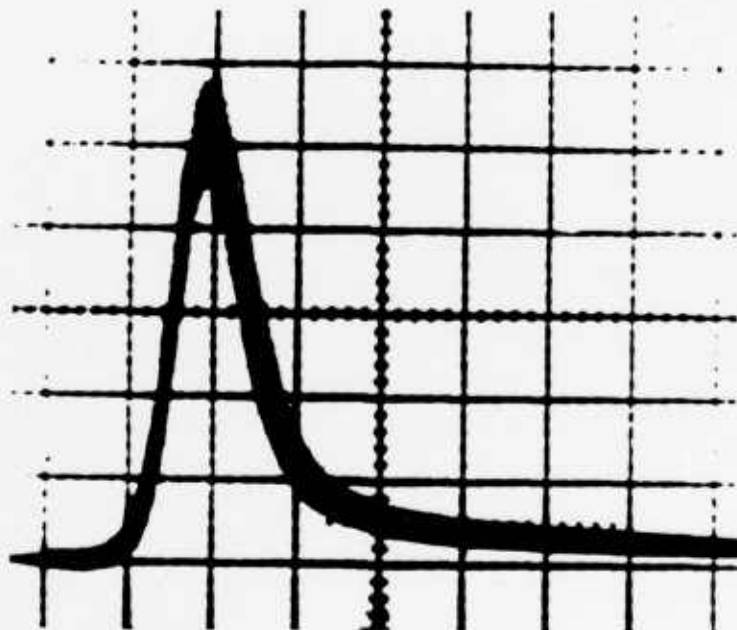


Figure 21  
Temporal Profile (Pulse Duration is 20 ns, FWHM)

Periodically, a complete two-dimensional analysis of the spatial profile is performed with a BEAMCODE diagnostics system using a silicon array camera and video frame grabber. The camera array is located precisely in the target plane or equivalent. Data acquired by the frame grabber are transferred to a computer for near real-time analysis of individual laser pulses.

Software permits quantitative determination of pulse energy and maximum fluence and provides graphic displays of the spatial profile in several formats (Figure 22). Independent verification of the radiation distribution in the target plane is obtained by scanning at that location with a pinhole and silicon photodiode. Figure 23 shows the excellent agreement between BEAMCODE measurements and pinhole scans. Numerical integration of this extremely Gaussian spatial profile yields the ratio of total pulse energy to maximum fluence in the target plane. This ratio is called the effective area. Shot-to-shot variation of effective area is typically less than 5%.

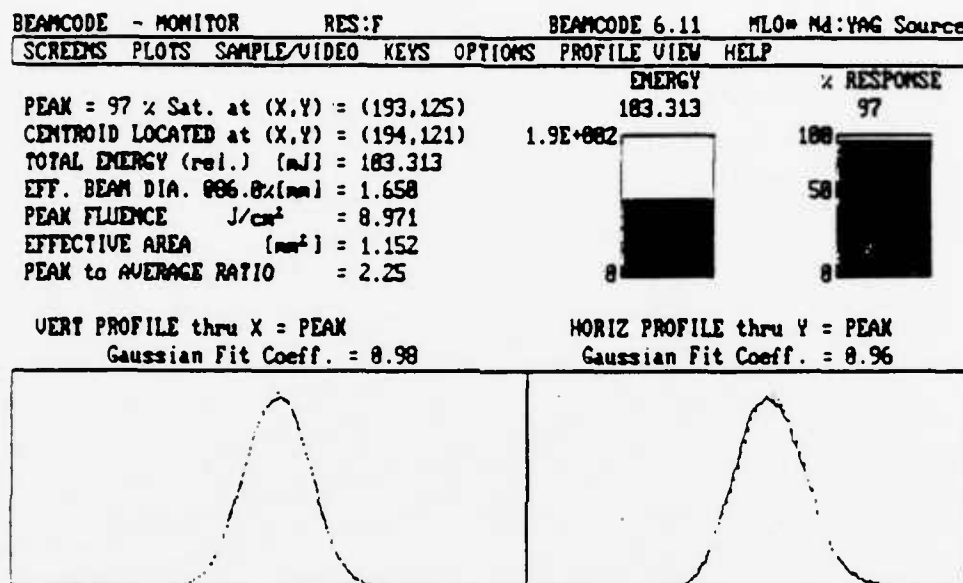


Figure 22  
Spatial Profile Obtained with Array Camera (Spot Size is 1.65 mm, FW1/e<sup>2</sup>)

### 3.2 Test Samples

The damage test station is equipped with a variety of interchangeable fixtures to permit mounting test samples of different geometries. When certifying laser damage resistance to a drawing or other procurement specification, it's preferable that actual laser optics, rather than witness samples, be tested to be assured of representative parts. Where used, witness samples usually are coated glass pieces, typically 1 inch in diameter by 3/8 inch thick. In most cases one surface (the entrance face) has been carefully polished and coated while the exit face is generally uncoated and has a commercial grade "window" polish. It's best that transmissive samples with an uncoated exit face have a 3 degree wedge. Pieces of unusual geometry occasionally require specialized holders to be fabricated.

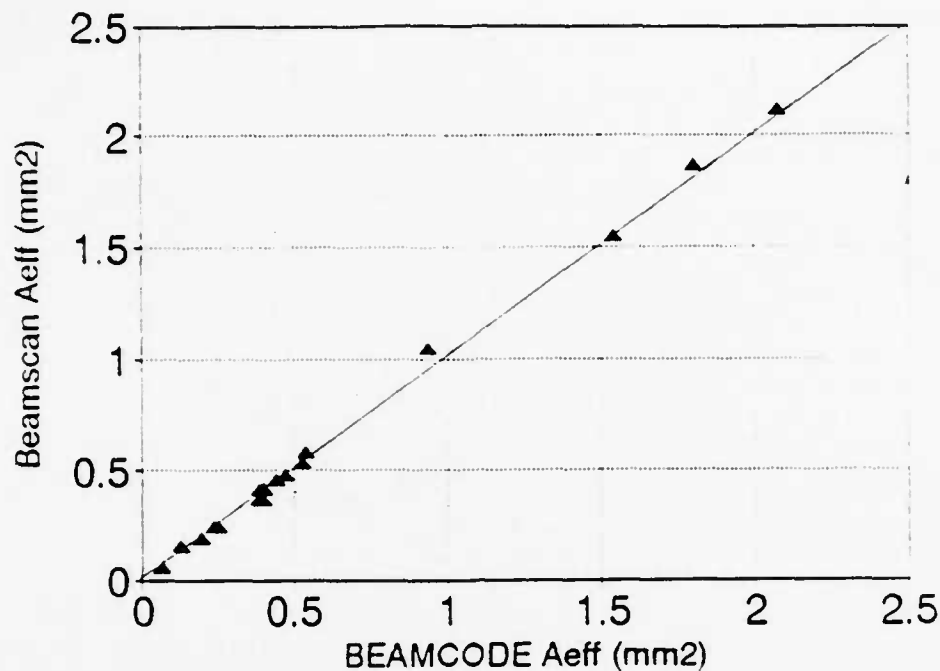


Figure 23  
Spatial Profile Comparison, BEAMCODE to Pinhole Scan

Before testing, any loose particulates are removed by applying a low-pressure stream of nitrogen gas, followed by drawing a lens tissue saturated with methanol, acetone or other high purity solvent across the test surface. More vigorous cleaning procedures are performed if required.

### 3.3 Exposure Test Procedures

There are five major types of laser exposure test: damage threshold, optical durability certification, transmission vs fluence, optical density and specialty (such as lifetime testing). The damage threshold and optical durability certification tests are described briefly here; variants are made depending upon the optic and test specifications.

*Damage Threshold.* "Damage" is usually defined as any permanent laser-induced change which is observable at high magnification with a differential interference contrast or dark field microscope. It may be defined differently if the application requires. "Threshold" is defined to be the lowest fluence sufficient to induce damage at any test site. To determine the damage threshold, a number of sample sites are irradiated at different fluences. Each site is observed immediately before, during, and after irradiation with the on-line 20X microscope, and any visible change, plasma

formation, or change in the scatter of the HeNe laser beam is noted. After exposure and if required by the test, the test sites are examined microscopically to confirm damage and characterize laser-induced changes. Color photomicrography in several formats is available.

The *Damage Frequency Method* is the standard damage threshold procedure specified by the International Standards Organization. The test sample is irradiated at several different fluence levels with a predetermined number of sites (usually 10) at each level. The levels are purposely chosen so that at the higher fluence levels a high probability of damage exists, whereas at the lower levels, a low probability of damage exists. The percentage of failures at each fluence is plotted against the fluence levels. A least squares linear fit to this data is calculated and the zero percent failure intercept defines the damage threshold level. A typical exposure data set is shown in Figure 24. This method provides the most accurate measurement of damage threshold but requires a relatively large sample, since many sites must be exposed.

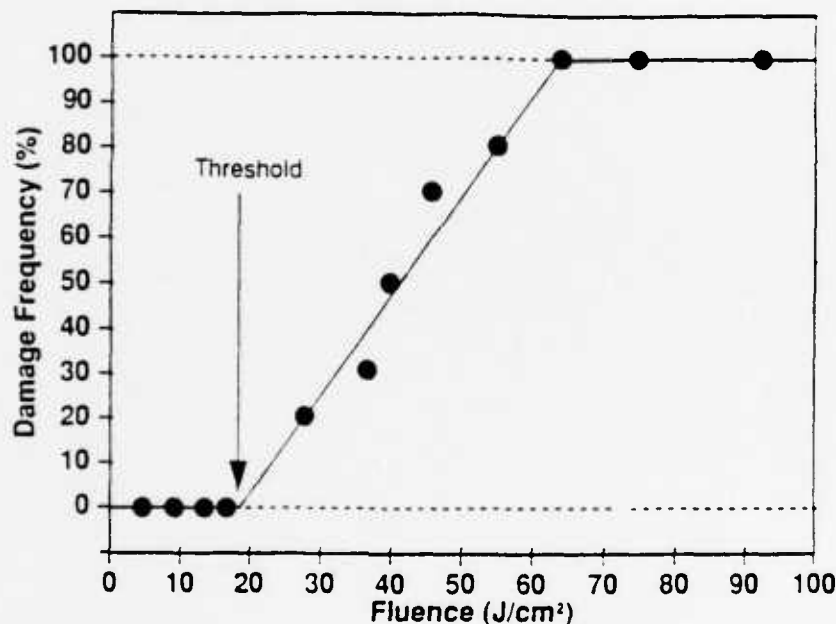


Figure 24  
Typical Damage Frequency Method Data

As before, the fluence levels are distributed approximately uniformly over a range including the anticipated failure level. One site is irradiated at each fluence level, and the *Least Fluence Failure* is taken as an estimate of the damage threshold. If untested sites remain, these are exposed at lower fluence levels for confirmation. A typical data set is shown in Figure 25. If the damage/no

damage overlap region is small, as shown, the least fluence failure estimates the damage threshold with good confidence.

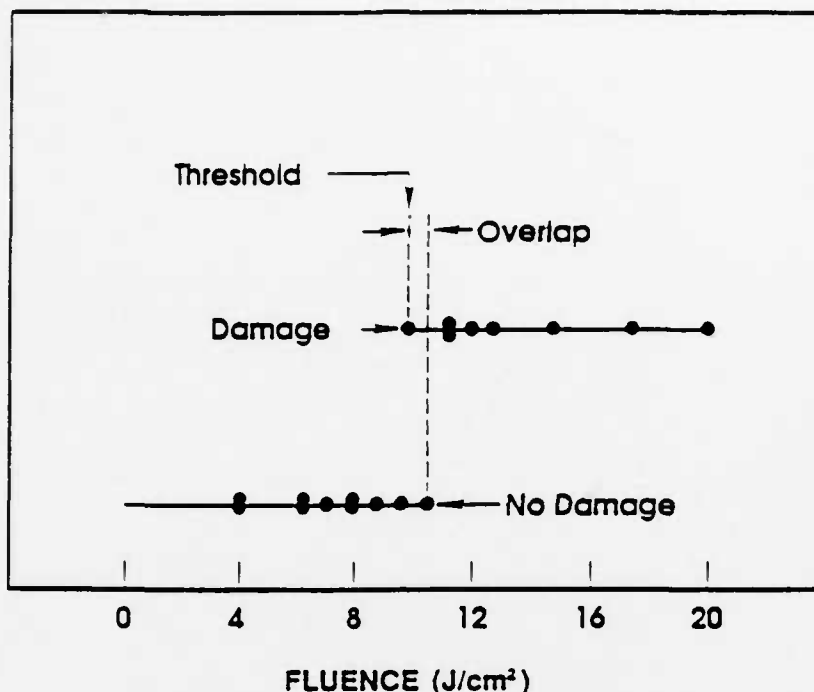


Figure 25  
Typical Least Fluence Failure Method Data

On most laser optics, the surface damage threshold is defect driven, meaning it will fail at weak, isolated sites. If these sites are close together compared to the test beam size, relatively few test sites are needed to determine the damage threshold. In this case, the damage frequency plot will yield a near vertical line and the least fluence data will have a small overlap. Conversely if the weak sites are widely separated compared to the test beam size, a low slope and a large overlap will result.

Several test sites (usually chosen on a uniform grid and sampling a representative surface area) are exposed to laser radiation at one specified combination of fluence, repetition rate, pulse duration, spot size and minimum number of pulses per site. The sample is observed as before with the on-line 20X microscope and damage at any site constitutes "failure" in this test. This test is usually done on optics intended for use in laser hardware and seldom on witness samples. Results of the tests on POC's broadband IR filter are summarized below. Results at Site #2 are seen in Figures 26 and 27 and Table 5. Results at Site #1 are seen in Figures 28 and 29 and Table 6. Results at Site #3 are seen in Figures 30 and 31 and Table 7.



Figure 28  
Illustration of Laser Damage Threshold Test of POC's Broadband IR Samples. The damage was  
observed when energy exceeded  $10.2 \text{ J/cm}^2$  at an angle of  $0^\circ$

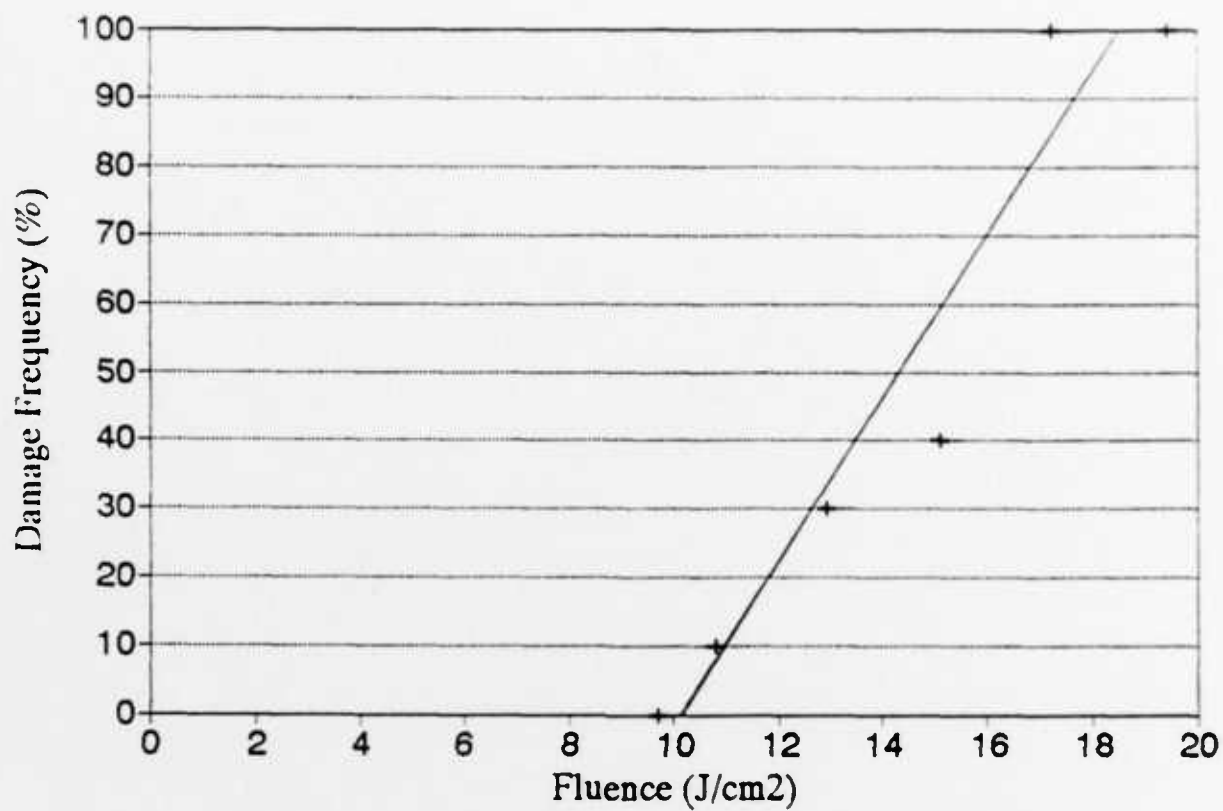


Figure 27  
Physical Optics Holographic Filter Tested on Hologram Side, Site #2, 0 deg

### Regression Output:

Constant	-121.707
Std Err of Y Est	14.5948
R Squared	0.895584
No. of Observations	5
Degrees of Freedom	3
X Coefficient(s)	11.97024
Std Err of Coef.	2.359783

Pit formation on hologram layer only during first few pulses. May continue to propagate at higher fluences.



**LASER DAMAGE THRESHOLD**

**820 MW/cm<sup>2</sup> or 10.2 J/cm<sup>2</sup>**

Cert. No.: 03/10/92 Q2  
Work Order No.: 2766

Supplier: Physical Optics Corp.  
Lot: Holographic Filter 9-10-10

Special Requirements: Incident on hologram side, site #2

**TEST CONDITIONS**

Substrate: Float Glass	Coating: Filter (holographic)
Wavelength: 1064 nm	Incidence: 0°
Repetition Freq: 20 Hz	Spot Size (FW1/e <sup>2</sup> ): 1.05 mm
Pulse Width (FWHM): 10 ns	Polarization State: Linear
Axial Modes: Etalon-Limited (SPO)	Transverse Modes: TEM <sub>00</sub>
No. Sites: 48	No. Shots/Site: 200

Preparation: Acetone-methanol drag wipe  
Damage Definition: Permanent change to any layer  
Inspection Method: Online, Nomarski/Darkfield 150X  
Texture: Smooth  
Features: Few point scatter centers  
Scatter: Bright haze  
Damage Type: Pit formation on hologram layer

Note: Pits form during first few pulses. No damage noted on epoxy layer. Pits may continue to propagate at higher fluences.  
Threshold calculated by damage frequency method. Photos to follow.

*Montana Laser Optics, Inc. certifies that the Laser Damage Threshold of this sample was tested as shown. Fluence measurement precision was plus or minus 10% traceable to NIST. The test method was substantially in agreement with ISO 11254. Specific calibration data are maintained in this office and are available on request.*

*Ray Juma*

**MONTANA LASER OPTICS**  
**LASER DAMAGE TESTING**

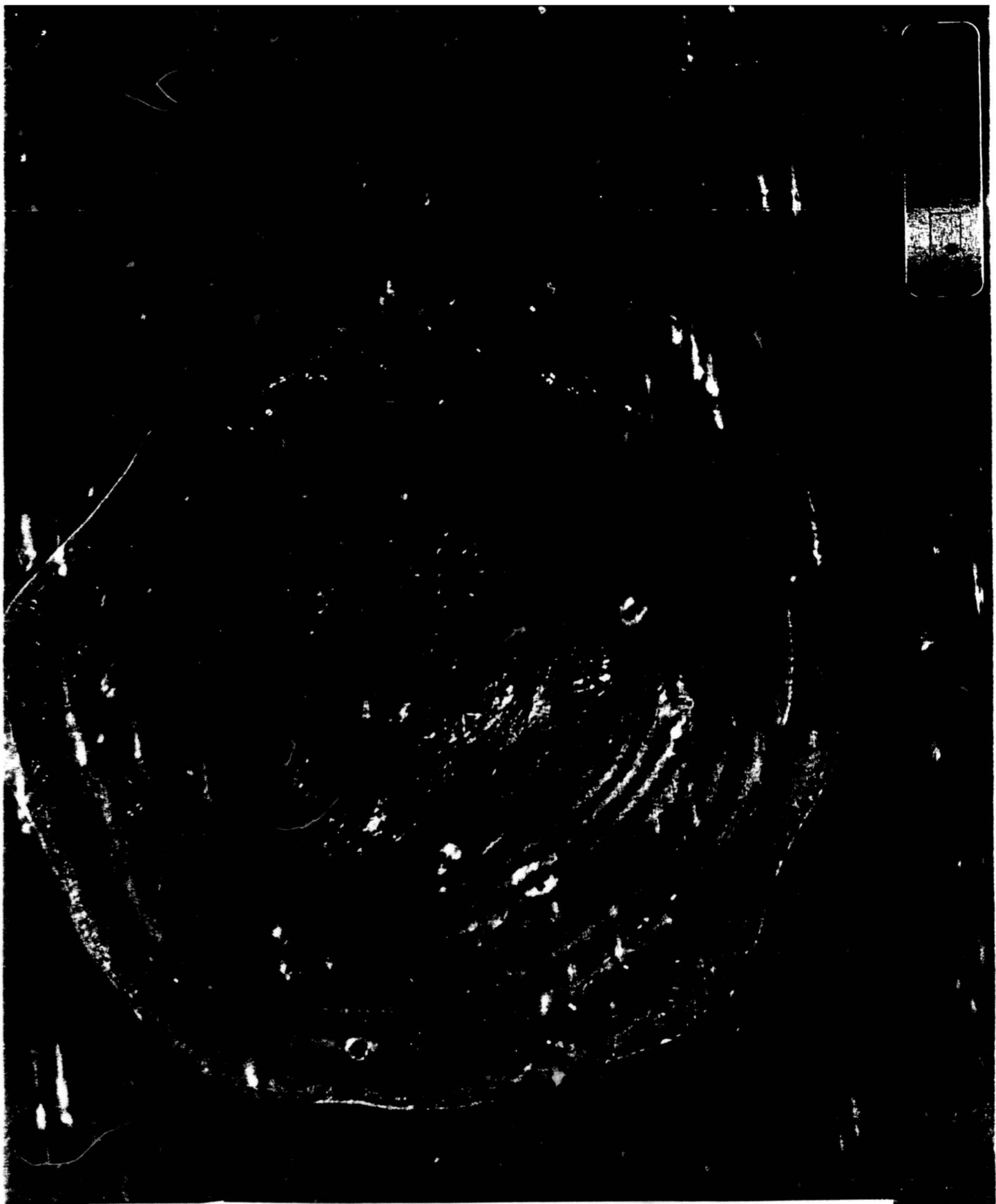


Figure 28  
Illustration of Laser Damage to POC's Broadband IR Filter. The damage was observed after exposure energy exceeded  $2.6 \text{ J/cm}^2$  at an angle of  $0^\circ$ . (5X Objective)

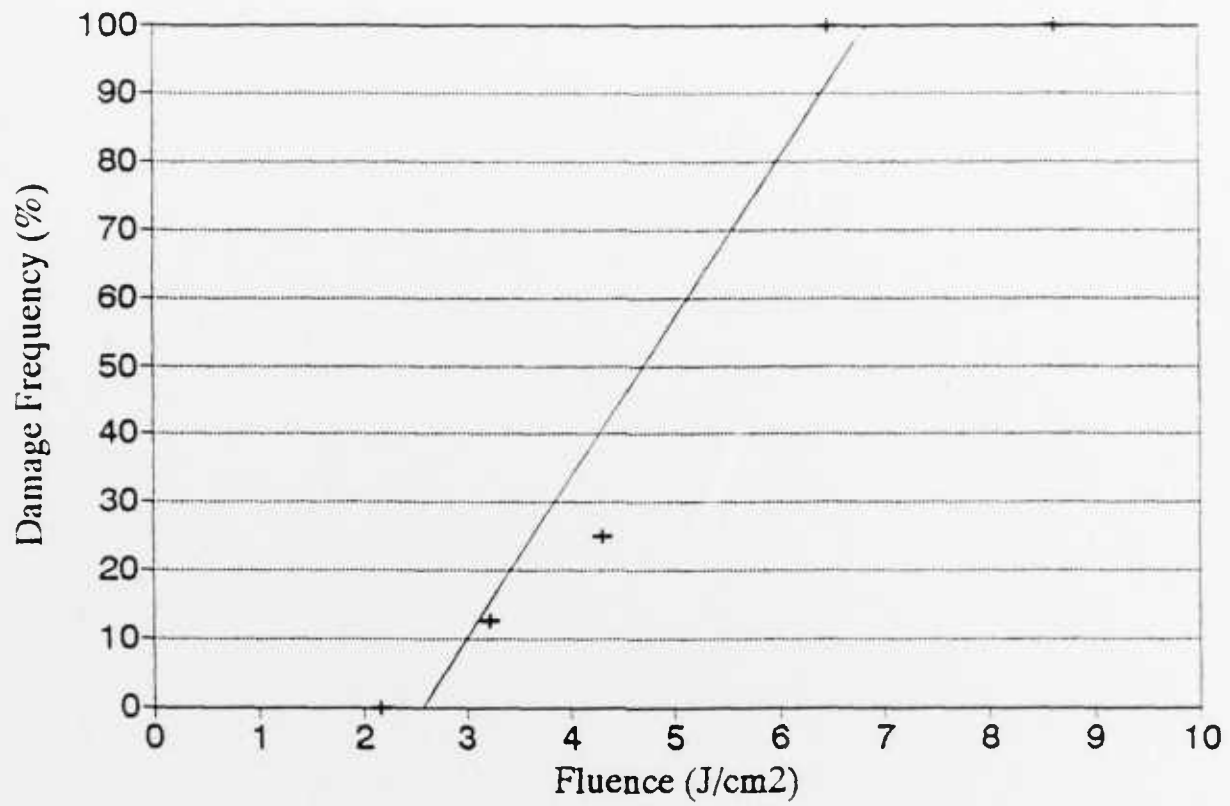


Figure 29  
Physical Optics Holographic Filter Exposure Incident on Epoxy Side, Site #1

Table 6. Measurement of Laser Damage Threshold for Site #1

Energy (mJ)	Fluence (J/cm <sup>2</sup> )	Sites	Fail	%Fail	LS Fit
THRESH	2.6				-0.0
SAT	6.8				100.0
10	2.2	8	0	0	-10.0
15	3.2	8	1	12.5	15.4
20	4.3	8	2	25	40.7
30	6.5	8	8	100	91.4
40	8.6	8	8	100	142.1
50	10.8	8	8	100	192.9
60	13.0	6	6	100	243.6
	0.0	0	0	ERR	-60.7
	0.0	0	0	ERR	-60.7
	0.0	0	0	ERR	-60.7
	0.0	0	0	ERR	-60.7
	0.0	0	0	ERR	-60.7
	0.0	0	0	ERR	-60.7
	0.0	0	0	ERR	-60.7
		54	Total		

Regression Output:

Constant	-60.7143
Std Err of Y Est	14.6385
R Squared	0.929217
No. of Observations	4
Degrees of Freedom	2
X Coefficient(s)	23.48071
Std Err of Coef.	4.582512

Notes: Exposure incident on epoxy side,  
Site #1, 0 deg angle of incidence.  
Extrapolated failure level of 2.6 J/cm<sup>2</sup> reported.

Small pit formation on epoxy layer which continue  
to form throughout pulse train. Some pitting noted  
on hologram layer at higher fluences.

**LASER DAMAGE THRESHOLD**

**210 MW/cm<sup>2</sup> or 2.6 J/cm<sup>2</sup>**

Cert. No.: 03/10/92 Q1  
Work Order No.: 2766

Supplier: Physical Optics Corp.  
Lot: Holographic Filter 9-10-10

Special Requirements: Incident on epoxy side, site #1

**TEST CONDITIONS**

Substrate: Float Glass	Coating: Filter (holographic)
Wavelength: 1064 nm	Incidence: 0°
Repetition Freq: 20 Hz	Spot Size (FW1/e <sup>2</sup> ): 1.05 mm
Pulse Width (FWHM): 10 ns	Polarization State: Linear
Axial Modes: Etalon-Limited (SPO)	Transverse Modes: TEM <sub>00</sub>
No. Sites: 54	No. Shots/Site: 200

Preparation: Acetone-methanol drag wipe  
Damage Definition: Permanent change to any layer  
Inspection Method: Online, Nomarski/Darkfield 150X  
Texture: Smooth  
Features: Few point scatter centers  
Scatter: Bright haze  
Damage Type: Small pit formation on epoxy layer

**Note:** Pits continue to form throughout pulse train. Some pitting noted on hologram layer at higher fluences. Threshold calculated by damage frequency method. Photos to follow.

*Montana Laser Optics, Inc. certifies that the Laser Damage Threshold of this sample was tested as shown. Fluence measurement precision was plus or minus 10% traceable to NIST. The test method was substantially in agreement with ISO 11254. Specific calibration data are maintained in this office and are available on request.*

  
**MONTANA LASER OPTICS**  
**LASER DAMAGE TESTING**

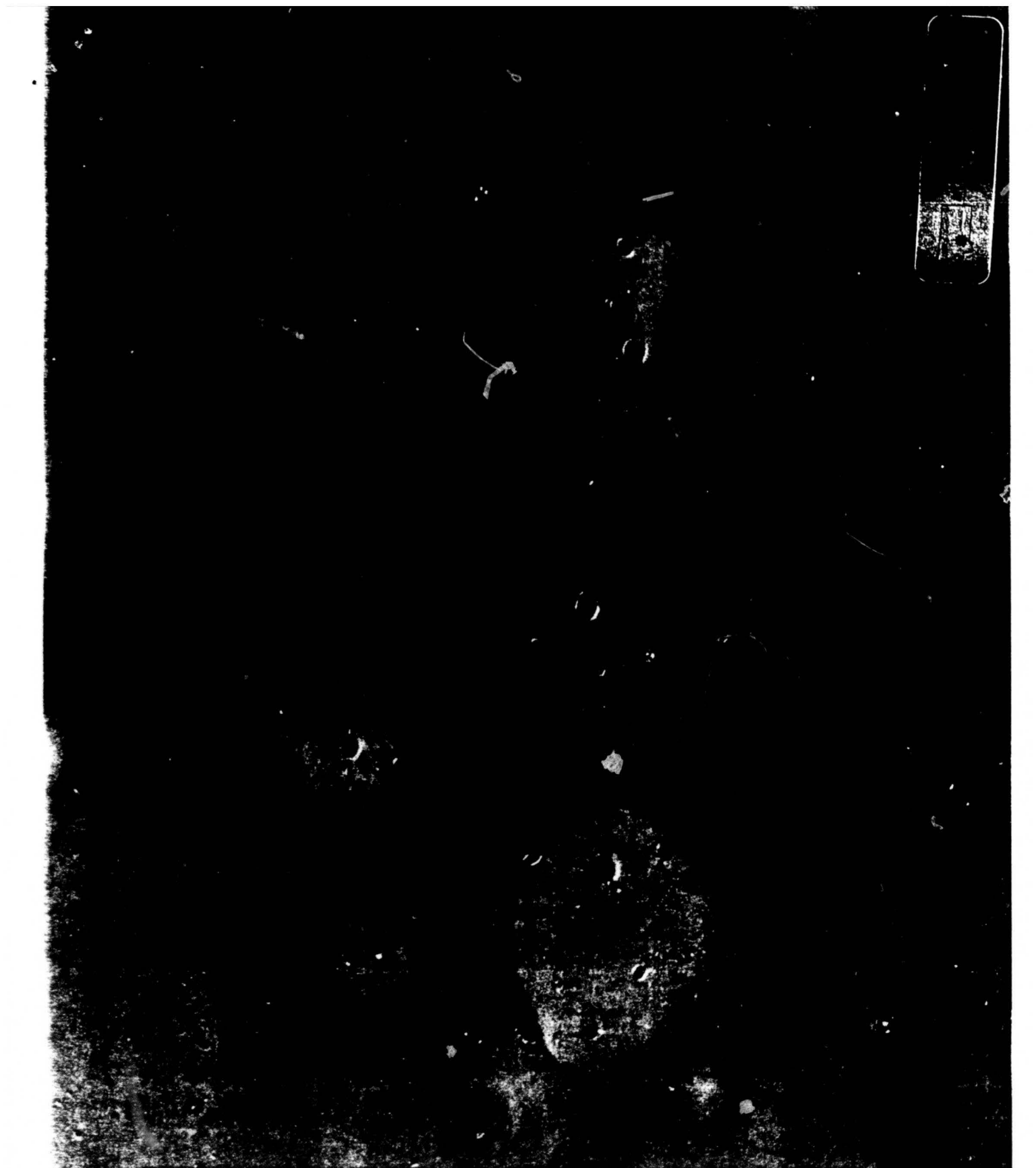


Figure 30  
Illustration of Damage to POC's Broadband IR Filter at Exposure Levels Above  $2.2 \text{ J/cm}^2$  at an angle of  $30^\circ$

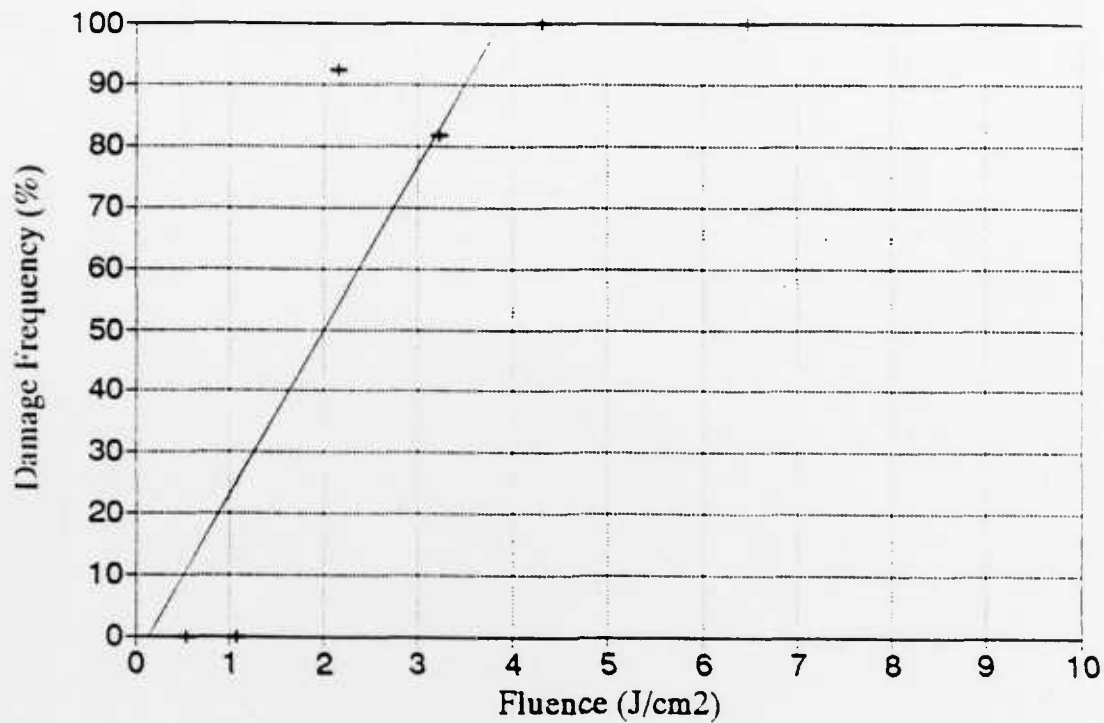


Figure 31  
Physical Optics Holographic Filter Tested on Hologram Side, Site #3, 30 deg

Table 7. Laser Damage Threshold Measurement for Site #3

Energy (mJ)	Fluence (J/cm <sup>2</sup> )	Sites	Fail	%Fail	LS Fit
THRESH	0.1				-0.0
SAT	3.9				100.0
2.5	0.5	3	0	0	10.6
5	1.1	3	0	0	25.1
10	2.2	13	12	92.30769	54.1
15	3.2	11	9	81.81818	83.0
20	4.3	3	3	100	112.0
30	6.5	3	3	100	169.9
50	10.8	4	4	100	285.7
70	15.1	6	6	100	401.5
90	19.4	2	2	100	517.3
	0.0	0	0	ERR	-3.8
	0.0	0	0	ERR	-3.8
	0.0	0	0	ERR	-3.8
	0.0	0	0	ERR	-3.8
		48	:	Total	

Regression Output:

Constant	-3.84615
Std Err of Y Est	33.45041
R Squared	0.651894
No. of Observations	4
Degrees of Freedom	2
X Coefficient(s)	26.80867
Std Err of Coef.	13.85248

Notes: Exposure incident on hologram side,  
Site #3, 30 deg angle of incidence.  
Least fluence failure of 2.2 J/cm<sup>2</sup> reported.

Many small pits which form on exit surface of epoxy  
layer (leaves a beam "footprint"). High transmission  
noted at 30 deg angle of incidence.



**LASER DAMAGE THRESHOLD**

**180 MW/cm<sup>2</sup> or 2.2 J/cm<sup>2</sup>**

Cert. No.: 03/10/92 Q3  
Work Order No.: 2766

Supplier: Physical Optics Corp.  
Lot: Holographic Filter 9-10-10

Special Requirements: Incident on hologram side, site #3

**TEST CONDITIONS**

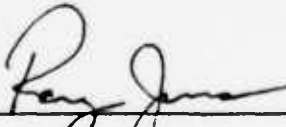
Substrate: Float Glass  
Wavelength: 1064 nm  
Repetition Freq: 20 Hz  
Pulse Width (FWHM): 10 ns  
Axial Modes: Etalon-Limited (SPO)  
No. Sites: 48

Coating: Filter (holographic)  
Incidence: 30°  
Spot Size (FW1/e<sup>2</sup>): 1.05 mm  
Polarization State: Linear  
Transverse Modes: TEM<sub>00</sub>  
No. Shots/Site: 200

Preparation: Acetone-methanol drag wipe  
Damage Definition: Permanent change to any layer  
Inspection Method: Online, Nomarski/Darkfield 150X  
Texture: Smooth  
Features: Few point scatter centers  
Scatter: Bright haze  
Damage Type: Small pit formation on exit surface of epoxy layer

Note: Threshold value is relative to plane at normal incidence. Pits form on exit surface of epoxy layer (leaves a beam "footprint"). Threshold is least-fluence failure. Photos to follow. High transmission noted.

*Montana Laser Optics, Inc. certifies that the Laser Damage Threshold of this sample was tested as shown. Fluence measurement precision was plus or minus 10% traceable to NIST. The test method was substantially in agreement with ISO 11254. Specific calibration data are maintained in this office and are available on request.*



**MONTANA LASER OPTICS**  
**LASER DAMAGE TESTING**

During the second year of this program, we will complete all of the remaining or partially completed tasks.

#### 4.0 REFERENCES

1. J. Jansson, T. Jansson, and K. Yu, "Solar Control Tunable Lippmann Holowindow," *Solar Energy Material*, 14, 289 (1986).
2. T. Jansson, I. Tengara, Y. Qiao, and G. Savant, "Lippmann-Bragg Broadband Holographic Mirrors," *JOSA*, 8(1), 201-211 (1991).
3. E. Kogelnik, *Bell Syst. Tech. J.*, 24, 244 (1968).